APPENDICES

APPENDIX I

a) Eigenvalue equation to obtain u_g and v_g

$$\begin{pmatrix} I & -R \\ 0 & MT \end{pmatrix} \begin{pmatrix} u \\ v \end{pmatrix} = e^{-ik_z d_z} \begin{pmatrix} TP & 0 \\ -MRP & I \end{pmatrix} \begin{pmatrix} u \\ v \end{pmatrix}$$

where, $M_{g,g'} = e^{-i\vec{g}.\vec{d}_i} e^{i\vec{K}'_{gx} d_x} \delta_{g,g'}$ and $P_{g,g'} = e^{i\vec{g}.\vec{d}_i} e^{i\vec{K}'_{gx} d_x} \delta_{g,g'}$

d is a lattice translation vector, R and T are the reflection and transmission matrices between the layers and their expressions have been given by Pendry[36].

b) Expressions for $B_l(r)$ and $D_l(r)$, the radial part of the photon field for different values of l

$$B_0(r) = 2\int_0^{\pi} \frac{P_0(\cos\theta)}{\frac{r}{a}\cos\theta + \beta_1} \sin\theta d\theta$$

$$= \frac{2a}{r} \ln\left[\frac{\frac{r}{a} + \beta_1}{-\frac{r}{a} + \beta_1}\right]$$

$$B_1(r) = \frac{2}{3}\int_0^{\pi} \frac{P_1(\cos\theta)\sin\theta d\theta}{\frac{r}{a}\cos\theta + \beta_1}$$

$$= \frac{2}{3}\left[\frac{2a}{r} - \beta_1 \left(\frac{a}{r}\right)^2 \frac{\frac{r}{a} + \beta_1}{-\frac{r}{a} + \beta_1}\right]$$

$$B_2(r) = \frac{2}{5}\int_0^{\pi} \frac{P_2(\cos\theta)\sin\theta d\theta}{\frac{r}{a}\cos\theta + \beta_1}$$

$$= \frac{2}{5}\left[-3\beta_1 \left(\frac{a}{r}\right)^2 + \frac{3}{2}\beta_1^2 \left(\frac{a}{r}\right)^3 \ln\frac{\frac{r}{a} + \beta_1}{-\frac{r}{a} + \beta_1} - \frac{a}{2r} \ln\frac{\frac{r}{a} + \beta_1}{-\frac{r}{a} + \beta_1}\right]$$

$$B_3(r) = \frac{2}{7}\int_0^{\pi} \frac{P_3(\cos\theta)\sin\theta d\theta}{\frac{r}{a}\cos\theta+\beta_1}$$

$$=\frac{1}{7}\left[5\left\{\frac{2a}{3r}+2\left(\frac{a}{r}\right)^3\beta_1^2-\beta_1^3\left(\frac{a}{r}\right)^4\ln\frac{\frac{r}{a}+\beta_1}{-\frac{r}{a}+\beta_1}\right\}-\frac{15}{2}B_2(r)\right]$$

$$B_4(r) = \frac{2}{9}\int_0^{\pi} \frac{P_4(\cos\theta)\sin\theta d\theta}{\frac{r}{a}\cos\theta+\beta_1}$$

$$=\frac{1}{36}\left[35\left\{-\frac{2}{3}\beta_1\left(\frac{a}{r}\right)^2-2\beta_1^3\left(\frac{a}{r}\right)^4+\beta_1^4\left(\frac{a}{r}\right)^5\ln\frac{\frac{r}{a}+\beta_1}{-\frac{r}{a}+\beta_1}\right\}\right.$$

$$-30\left\{-2\beta_1^3\left(\frac{a}{r}\right)^2+\beta_1^2\left(\frac{a}{r}\right)^3\ln\frac{\frac{r}{a}+\beta_1}{-\frac{r}{a}+\beta_1}\right\}$$

$$\left.+3\frac{a}{r}\ln\frac{\frac{r}{a}+\beta_1}{-\frac{r}{a}+\beta_1}\right]$$

$$D_0(r) = 2\int_0^{\pi} \frac{P_0(\cos\theta)\sin\theta d\theta}{\left(\frac{r}{a}\cos\theta+\beta_1\right)^2}$$

$$=-\frac{2}{\beta_1^2-\frac{r^2}{a^2}}$$

$$D_1(r) = \frac{2}{3}\int_0^{\pi} \frac{P_1(\cos\theta)\sin\theta d\theta}{\left(\frac{r}{a}\cos\theta+\beta_1\right)^2}$$

$$=\frac{2a}{3r}\left[-\frac{2\beta_1}{\beta_1^2-\frac{r^2}{a^2}}+\frac{a}{r}\ln\frac{\frac{r}{a}+\beta_1}{-\frac{r}{a}+\beta_1}\right]$$

$$D_2(r) = \frac{2}{5}\int_0^{\pi} \frac{P_2(\cos\theta)\sin\theta\, d\theta}{(\frac{r}{a}+\beta_1)^2}$$

$$= \frac{2}{5}\Big[\frac{3}{2}\Big\{2(\frac{a}{r})^2+2\beta_1(\frac{a}{r})^2\frac{1}{\beta_1^2-\frac{r^2}{a^2}}$$

$$-2\beta_1(\frac{a}{r})^3\ln\frac{\frac{r}{a}+\beta_1}{-\frac{r}{a}+\beta_1}\Big\}-\frac{1}{\beta_1^2-\frac{r^2}{a^2}}\Big]$$

$$D_3(r) = \frac{2}{7}\int_0^{\pi} \frac{P_3(\cos\theta)\sin\theta\, d\theta}{(\frac{r}{a}+\beta_1)^2}$$

$$=\Big[-4\beta_1(\frac{a}{r})^3-2\beta_1^3(\frac{a}{r})^3\frac{1}{\beta_1^2-\frac{r^2}{a^2}}$$

$$+3\beta_1^2(\frac{a}{r})^4\ln\frac{\frac{r}{a}+\beta_1}{-\frac{r}{a}+\beta_1}\Big]$$

$$D_4(r) = \frac{2}{9}\int_0^{\pi} \frac{P_4(\cos\theta)\sin\theta\, d\theta}{(\frac{r}{a}\cos\theta+\beta_1)^2}$$

$$=\frac{1}{36}\Big[35\Big\{\frac{2}{3}(\frac{a}{3})^2+6\beta_1^2(\frac{a}{r})^4+2\beta_1^4(\frac{a}{r})^4\frac{1}{\beta_1^2-\frac{r^2}{a^2}}-4\beta_1^3(\frac{a}{r})^5\ln\frac{\frac{r}{a}+\beta_1}{-\frac{r}{a}+\beta_1}\Big\}$$

$$-30\Big\{2(\frac{a}{r})^2+2\beta_1^2(\frac{a}{r})^2\frac{1}{\beta_1^2-\frac{r^2}{a^2}}-2\beta_1(\frac{a}{r})^3\ln\frac{\frac{r}{a}+\beta_1}{-\frac{r}{+}\beta_1}\Big\}+\frac{6}{\beta_1^2-\frac{r^2}{a^2}}\Big]$$

APPENDIX II

```
C       PHOTOEMISSION PROGRAM WITH FREE ELECTRON WAVEFUNCTION
        COMPLEX A1,B1,CI,T1,T2,T3,T4,EPS,CMPLX
        COMMON AKI,AKP,AKF,AQ,A,ALPHA,CI
        CI=(0.,1.)
        READ (1,*) NP,NINT
        READ(1,*)WP,EI,THETA,A,ALPHA,VZ,NE
        WRITE(NP,4) WP,EI,THETA,A,ALPHA,VZ
        AKI=SQRT(2.*EI)
        AKP=SQRT(2.*(VZ-EI))
        DO 99 IE=1,NE
        READ(1,*) W,EPS1,EPS2
        AKF=SQRT(2.*(EI+W))
        AQ=SQRT(2.*(EI+W-VZ))
        WRITE(NP,2) W,AKI,AKP,AKF,AQ
        EPS=CMPLX(EPS1,EPS2)
        CALL REFRAC(W,WP,THETA,EPS,A1,B1)
        CALL TERM1 (A1,T1)
        CALL TERM2 (A1,B1,EPS,T2,NINT)
        CALL TERM3 (A1,EPS,T3)
        CALL TERM4 (A1,B1,EPS,T4,NINT)
        WRITE(NP,3) W,T1,T2,T3,T4
        CUR=CABS(T1+T2+T3+T4)
        CUR=CUR*CUR*AKF*AKF/W
 99     WRITE(NP,5)W,EPS,CUR
  2     FORMAT(3X,5(E12.4,3X))
  3     FORMAT(1X,F7.3,8(2X,E10.3))
  4     FORMAT(15X,6F12.4)
  5     FORMAT(2X,'W=',F7.4,'EPS=',2F10.4,'CURRENT=',E12.4)
        STOP
        END
C
         SUBROUTINE TERM3(A1,EPS,T3)
         COMPLEX A1,R1,CI,T3,EPS,Q,R2
         COMMON AKI,AKP,AKF,AQ,A,ALPHA,CI
         Q=SQRT(AKI/AQ) *AKP*EPS
         R2=1./(AKP-CI*AQ)
         R1=1./(CI*AQ+AKP)
         T3=R1+R2*(AQ-AKF)/(AQ+AKF)
         T3=-Q*T3*CI
         T3=T3*A1/(-AKP+CI*AKI)
         RETURN
         END
C
        SUBROUTINE TERM1(A1,T1)
         COMPLEX A1,T1,C1,C2,CI
         COMMON AKI,AKP,AKF,AQ,A,ALPHA,CI
         Q=SQRT(AKI*AQ)
         Q=0.5*Q/(AQ+AKF)
         AH=A*(AKI-AKF)
         C1=COS(AH)-CI*SIN(AH)
         C1=C1*EXP(-ALPHA*A)/(ALPHA+CI*(AKI-AKF))
         AG=A*(AKI+AKF)
         C2=COS(AG)+CI*SIN(AG)
```

```
      C2=C2*(CI*AKI+AKP)/(CI*AKI-AKP)
      C2=C2*EXP(-ALPHA*A)/(ALPHA-CI*(AKI+AKF))
      T1=2.*CI*A1*Q*(C1-C2)
      RETURN
      END
C
      SUBROUTINE TERM2 (A1,B1,EPS,T2,NINT)
      COMPLEX A1,B1,EPS,T2,CI,F1,F2,R1,R2,Q
      DIMENSION F1(1001),F2(1001)
      COMMON AKI,AKP,AKF,AQ,A,ALPHA,CI
      Q=CI*A*A1*EPS*SQRT(AQ*AKI)/(AQ+AKF)
      AL=-A
      AH=0.
      D=(AH-AL)/(NINT-1)
      DO 10 I=1,NINT
      X=AL+(I-1)*D
      F1(I)=COS((AKI-AKF)*X)+CI*SIN((AKI-AKF)*X)
      F1(I)=F1(I)*EXP(ALPHA*X)/(B1*X+A)
      F2(I)=COS((AKI+AKF)*X)-CI*SIN((AKI-AKF)*X)
10    F2(I)=F2(I)*EXP(ALPHA*X)/(B1*X+A)
      CALL SINT (AL,AH,F1,NINT,R1)
      CALL SINT (AL,AH,F2,NINT,R2)
      T2=R1-R2*(AKP+CI*AKI)/(CI*AKI-AKP)
      T2=Q*T2
      RETURN
      END
C
      SUBROUTINE TERM4 (A1,B1,EPS,T4,NINT)
      COMPLEX A1,B1,EPS,T4,F1,F2,R1,R2,Q
      DIMENSION F1(1001),F2(1001)
      COMMON AKI,AKP,AKF,AQ,A,ALPHA,CI
      Q=-0.5*B1*A1*A*EPS*SQRT(AQ/AKI)/(AQ+AKF)
      AL=-A
      AH=0.
      D=(AH-AL)/(NINT-1)
      DO 10 I=1,NINT
      X=AL+(I-1)*D
      F1(I)=COS((AKI-AKF)*X)+CI*SIN((AKI-AKF)*X)
      F2(I)=COS((AKI+AKF)*X)-CI*SIN((AKI+AKF)*X)
      F1(I)=F1(I)*EXP(ALPHA*X)/((B1*X+A)**2)
10    F2(I)=F2(I)*EXP(ALPHA*X)/((B1*X+A)**2)
      CALL SINT (AL,AH,F1,NINT,R1)
      CALL SINT (AL,AH,F2,NINT,R2)
      T4=R1+R2*(CI*AKI+AKP)/(CI*AKI-AKP)
      T4=Q*T4
      RETURN
      END
```

APPENDIX III

```
$DEBUG
CPHOTOEMISSION program with band wavefunction
      DIMENSION U(9),V(9),X(200),ATP(200),YGP(25),YGM(25),F2(200)
      DIMENSION YGFP(25),YGFM(25),YK(25),YH1(9,25),YH2(9,25)
      DIMENSION YH3(9,25),YH4(9,25),FR0(5),D4(5,200),D5(5,200)
      DIMENSION ZP(4,4,4,4),WP(4,4,4),VP(4,4,4),EPKF1(9),EMKF1(9)
      DIMENSION  PQ(2,9),PQF(2,9),IPQF(2,9),PKZ(9),XP(4,4,4,4)
      DIMENSION AR1(2),AR2(2),B1(2),B2(2),YP(4,4,4,4),F(200)
      DIMENSION A2(5,200),A3(5,200),E1(5,200),F1(200),F3(200)
      COMPLEX A2,A3,E1,FR0,CT1,CTM,ST1,STM,CF1,UX,UY,ZP,WP,VP
      COMPLEX EPS,EMKF1,U,V,CMPLX,CEXP,YK,YGP,YGM,YGFP,YGFM,EPKF1
      COMPLEX XA,YA,CT,ST,CF,A1,AB1,F1,F2,F3,F,XP,YP,PKZ
      COMPLEX EXKF,CSQRT,CI,YH1,YH2,YH3,YH4,CTP,STP,EPKF
      COMPLEX T1,T3,T4,T6,T8,T9,T10,CUR1,CUR2,EP2,D4,D5,EMKF
      COMMON/X1/R0,DD,TV
      COMMON/X2/AKF,AKP,AQ,ALPHA,PKZ,EXKF,AQKF
      COMMON/X3/U,V,E,EMKF1,YH1,YH2,YH3,YH4,YK,SQE,A1,AB1,FR0,
     &EPKF1,AD
      COMMON/X4/D4,D5,A2,A3,E1
      COMMON/X5/X,ATP,Z,CL,EE,NMESH,KRMT,JRKI,NF,INDP,IP
      COMMON/X6/F1,F2,F3,F,XP,YP,ZP,WP,VP
      DATA CZ,CI,PI/(0.0,0.0),(0.0,1.0),3.14159265/
      READ(1,*)Z,LMAX,R0
      READ(1,*)N,NINT,NMESH,NF,KRMT,INDP,IP
      READ(1,*)E,THETA,ALPHA,VZ,NW
      AKP=SQRT(2.*(VZ-E))
      SQE=SQRT(2.*E)
      READ(2,73)(X(J),ATP(J),J=1,NMESH)
 73   FORMAT(2E14.6)
      VPI=0.0
      DD=7.65306
      AD=R0+DD/4.
      AR1(1)=DD/2
      AR1(2)=DD/2
      AR2(1)=-DD/2
      AR2(2)=DD/2
      TV=ABS(AR1(1)*AR2(2)-AR1(2)*AR2(1))
      RTV=2.0*PI/TV
      B1(1)=AR2(2)*RTV
      B1(2)=-AR2(1)*RTV
      B2(1)=-AR1(2)*RTV
      B2(2)=AR1(1)*RTV
      IPQF(1,1)=0
      IPQF(2,1)=0
      IPQF(1,2)=1
      IPQF(2,2)=0
      IPQF(1,3)=-1
      IPQF(2,3)=0
      IPQF(1,4)=0
      IPQF(2,4)=1
      IPQF(1,5)=0
      IPQF(2,5)=-1
      IPQF(1,6)=1
```

```
      IPQF(2,6)=1
      IPQF(1,7)=1
      IPQF(2,7)=-1
      IPQF(1,8)=-1
      IPQF(2,8)=1
      IPQF(1,9)=-1
      IPQF(2,9)=-1
      WRITE(*,101) N
      DO 1 J=1,N
      WRITE (*,101) IPQF(1,J),IPQF(2,J)
      PQF(1,J)=FLOAT(IPQF(1,J))
      PQF(2,J)=FLOAT(IPQF(2,J))
      PQ(1,J)=B1(1)*PQF(1,J)+B2(1)*PQF(2,J)
 1    PQ(2,J)=B1(2)*PQF(1,J)+B2(2)*PQF(2,J)
      I2=1
      I3=1
      AK2=FLOAT(I2-1)*DK
      AK3=FLOAT(I3-1)*DK
101   FORMAT(2I3)
      READ(3,33)(U(IG),IG=1,9)
      READ(3,33)(V(IG),IG=1,9)
33    FORMAT(2E12.4)
      LMX=LMAX+2
      LMMAX=(LMAX+3)**2
      CT=CMPLX(1.0,0.0)
      ST=CZ
      CF=CMPLX(1.0,0.0)
      CALL SPHRM4(YK,CT,ST,CF,3)
      CALL SPLM(LMAX,NINT)
      DO 99 IW=1,NW
      READ(1,*)W,EPS1,EPS2
      EPS=CMPLX(EPS1,EPS2)
      AKF=SQRT(2.*(E+W))
      AQ=SQRT(2.*(E+W-VZ))
      AQKF=AQ+AKF
      EXKF=CEXP(CI*AKF*R0)
      YA=CMPLX(2.*E,-2.0*VPI+0.0000001)
      YA=CSQRT(YA)
      DO 31 JG=1,N
      BK2=PQ(1,JG)+AK2
      BK3=PQ(2,JG)+AK3
      CA=BK2*BK2+BK3*BK3
      XA=CMPLX(2.0*E-CA,-2.0*VPI+0.0000001)
      XA=CSQRT(XA)
      PKZ(JG)=XA
      EP1=2.*E+AKF*AKF
      EP2=2.*AKF*XA
      EPKF=EP1-EP2
      EPKF=CSQRT(EPKF)
      EMKF=EP1+EP2
      EMKF=CSQRT(EMKF)
      EPKF1(JG)=EPKF
      EMKF1(JG)=EMKF
      BX1=0.0
      CF1=CMPLX(1.0,0.0)
```

```
      IF(CA-1.0E-7)3,3,2
 2    BX1=SQRT(CA)
      CF1=CMPLX(BK2/BX1,BK3/BX1)
 3    CT1=XA/YA
      UX=XA-AKF
      CTP=UX/EPKF
      ST1=BX1/YA
      STP=BX1/EPKF
      UY=-XA-AKF
      CTM=UY/EMKF
      STM=BX1/EMKF
      CALL SPHRM4(YGP,CT1,ST1,CF1,LMX)
      CALL SPHRM4(YGM,-CT1,ST1,CF1,LMX)
      CALL SPHRM4(YGFP,CTP,STP,CF1,LMX)
      CALL SPHRM4(YGFM,CTM,STM,CF1,LMX)
      DO 31 K=1,LMMAX
      YH1(JG,K)=YGP(K)
      YH2(JG,K)=YGM(K)
      YH3(JG,K)=YGFP(K)
 31   YH4(JG,K)=YGFM(K)
      CALL REFRAC(THETA,A1,AB1,EPS,AD,R0)
      CALL TERM1(T1,NINT,EPS)
      CALL TERM3(T3,N,EPS)
      CALL TERM9(T9)
      CALL TERM6(T6,NINT,LMAX,EPS,N)
      CALL TERM4(T4,LMAX,NINT,N,EPS)
      CALL TERM8(T8,N)
      CALL TERM10(T10,NINT,LMAX,N)
      ALP1=ALPHA*R0
      ALP2=ALPHA*(R0+DD/2)*2.
      ALP3=ALPHA*(R0+DD)*2.
      CUR1=T9-T8+T10
      CUR2=(EXP(-ALP1)*(T1-T4+T6))+T3
      C1=CABS(CUR1)
      C1=C1*C1
      C2=CABS(CUR2)
      C2=C2*C2
      C1=(EXP(-ALP2)+EXP(-ALP3))*C1
      CUR=C1+C2
      CUR=CUR*AKF*AKF/W
 91   FORMAT(1X,'CUR',E12.4,1X,'W=',F7.4)
      WRITE(4,91)CUR,W
      WRITE(4,129)
 129  FORMAT(/)
 99   CONTINUE
      STOP
      END
C
     SUBROUTINE SPLM(LMAX,NINT)
      DIMENSION XP(4,4,4,4),YP(4,4,4,4),ZP(4,4,4,4),VP(4,4,4)
      DIMENSION F1(200),F2(200),F3(200),F(200),WP(4,4,4)
      COMPLEX F1,F2,F3,F,XP,YP,S2,S3,S4,ZP,S5,S6,WP,VP
      COMMON/X6/F1,F2,F3,F,XP,YP,ZP,WP,VP
      LM=LMAX+1
      DO 10 IL3=1,LM
```

```
      L3=IL3-1
      DO 10 IL2=1,LM+1
      L2=IL2-1
      DO 10 IL1=1,LM+1
      L1=IL1-1
      DO 10 M1=0,L1
      IM1=M1+1
      CALL PLM1(L1,M1,L2,L3,NINT,S2,S3,S4,S5,S6)
      YP(IL3,IL2,IL1,IM1)=S2
      XP(IL3,IL2,IL1,IM1)=S3
      ZP(IL3,IL2,IL1,IM1)=S4
      WP(IL3,IL1,IM1)=S5
      VP(IL3,IL1,IM1)=S6
10    CONTINUE
      RETURN
      END
C
      SUBROUTINE PLM1(L1,M1,L2,L3,NINT,S2,S3,S4,S5,S6)
      DIMENSION F2(200),F3(200),F1(200),F(200),F31(200),F21(200)
      DIMENSION XP(4,4,4,4),YP(4,4,4,4),ZP(4,4,4,4),WP(4,4,4)
      DIMENSION VP(4,4,4)
      COMPLEX F1,F2,F3,F,S2,S3,XP,YP,S4,ZP,F31,F21,S5,S6,WP,VP
      COMMON/X6/F1,F2,F3,F,XP,YP,ZP,WP,VP
      AL=0.
      AH=3.14159265
      C=(AH-AL)/(NINT-1)
      U=FLOAT((L3+M1)*(L3-M1+1))
      DO 1 K=1,NINT
      XN=AL+(K-1)*C
      X1=PLM(XN,L1,M1)
      IF(M1.GT.L3) THEN
      X2=0.
      ELSE
      X2=PLM(XN,L3,M1)
      ENDIF
      IF(M1+1.GT.L3) THEN
      X3=0.
      ELSE
      X3=PLM(XN,L3,M1+1)
      ENDIF
      X5=PLM(XN,L2,0)
      IF(M1-1.LT.0) THEN
      X4=0.
      ELSE
      X4=PLM(XN,L3,M1-1)
      ENDIF
      PX1=X1*X2
      PX2=X1*X3
      PX3=X1*X4*U
      S=SIN(XN)
      F3(K)=PX1*S*COS(XN)
      F31(K)=F3(K)*X5
      F2(K)=(PX2-PX3)*S*S
      F21(k)=F2(K)*X5
      F(K)=PX1*S*X5
```

```
 1    CONTINUE
      CALL SINT(AL,AH,F31,NINT,S3)
      CALL SINT(AL,AH,F21,NINT,S2)
      CALL SINT(AL,AH,F,NINT,S4)
      CALL SINT(AL,AH,F3,NINT,S5)
      CALL SINT(AL,AH,F2,NINT,S6)
      IF(CABS(S5).LE.1.0E-6) S5=0.
      IF(CABS(S6).LE.1.0E-6) S6=0.
      IF(CABS(S4).LE.1.0E-6) S4=0.
      IF(CABS(S3).LE.1.0E-6) S3=0.
      IF(CABS(S2).LE.1.0E-6) S2=0.
      RETURN
      END
C
      SUBROUTINE REFRAC(THETA,A1,B1,EPS,AD,R0)
      COMPLEX A1,CX,CSQRT,EPS,B1
      S2=SIN(2.*THETA)
      S1=SIN(THETA)
      C1=COS(THETA)
      B1=1./(1.-EPS)-R0/AD
      CX=EPS-S1*S1
      CX=CSQRT(CX)
      A1=-S2/(CX+EPS*C1)
      RETURN
      END
C
      SUBROUTINE TERM1(T1,NINT,EPS)
      DIMENSION F1(200),F2(200),U(9),V(9),F3(200),F(200),WP(4,4,4)
      DIMENSION PKZ(9),XP(4,4,4,4),YP(4,4,4,4),ZP(4,4,4,4),F4(200)
      DIMENSION YH1(9,25),YH2(9,25),YH3(9,25),YH4(9,25),YK(25)
      DIMENSION VP(4,4,4),EPKF1(9),EMKF1(9),FR0(5)
      COMPLEX F1,F2,EPS,R1,T1,U,V,CI,Q,EXKF,EMKF1,EPKF1,XP,YP,ZP
      COMPLEX YK,F3,CEXP,YH1,YH2,YH3,YH4,A1,AB1,Y,F,FR0,WP
      COMPLEX PKZ,F4,VP
      COMMON/X1/R0,DD,TV
      COMMON/X2/AKF,AKP,AQ,ALPHA,PKZ,EXKF,AQKF
      COMMON/X3/U,V,E,EMKF1,YH1,YH2,YH3,YH4,YK,SQE,A1,AB1,FR0,
     &EPKF1,AD
      COMMON/X6/F1,F2,F3,F,XP,YP,ZP,WP,VP
      CI=CMPLX(0.0,1.0)
      Q=(2.*AQ*A1*EPS)/(AQKF*(1.-EPS))
      Q=Q*TV*EXKF
      AL=-DD/4
      AH=R0
      C=(AH-AL)/(NINT-1)
      P1=SQE-AKF
      P2=-SQE-AKF
      DO 10 I=1,NINT
      X=AL+(I-1)*C
      Y=1./(X/AD+AB1)
      F1(I)=U(1)*CEXP(CI*P1*X)
      F2(I)=V(1)*CEXP(CI*P2*X)
      F3(I)=F1(I)-F2(i)
      F4(I)=F1(I)+F2(i)
 10   F(I)=F3(I)*(CI*SQE*Y)-0.5*Y*Y*F4(i)/AD
```

```
      CALL SINT(AL,AH,F,NINT,R1)
      T1=R1*Q
      RETURN
      END
C
      SUBROUTINE TERM3(T3,N,EPS)
      DIMENSION T(9),YH1(9,25),YH2(9,25),YH3(9,25),YH4(9,25),YK(25)
      DIMENSION U(9),V(9),FR0(5),PKZ(9),EPKF1(9),EMKF1(9)
      COMPLEX EPS,CI,T3,R1,R2,R,T,Q,EXKF,EMKF1,A1,AB1
      COMPLEX YH1,YH2,YH3,YH4,YK,U,V,FR0,EPKF1,PKZ
      COMMON/X1/R0,DD,TV
      COMMON/X2/AKF,AKP,AQ,ALPHA,PKZ,EXKF,AQKF
      COMMON/X3/U,V,E,EMKF1,YH1,YH2,YH3,YH4,YK,SQE,A1,AB1,FR0,
     &EPKF1,AD
      CI=CMPLX(0.0,1.0)
      Q=A1*EPS*AKP
      R1=1./(AKP+CI*AQ)
      R2=(AQ-AKF)/(AQKF)
      R2=R2/(AKP-CI*AQ)
      R=R1+R2
      CALL TG(T,N)
      T3=Q*T(1)*R*TV
      T3=-T3
      RETURN
      END
C
      SUBROUTINE TG(T,N)
      DIMENSION U(9),V(9),T(9),YK(25),FR0(5),PKZ(9),EPKF1(9)
      DIMENSION YH1(9,25),YH2(9,25),YH3(9,25),YH4(9,25)
      DIMENSION ZK(9),ENKF1(9)
      COMPLEX T,CI,U,V,EXKF,EMKF1
      COMPLEX YK,YH1,YH2,YH3,YH4,A1,AB1,FR0,EPKF1,PKZ,ZK
      COMMON/X1/R0,DD,TV
      COMMON/X2/AKF,AKP,AQ,ALPHA,PKZ,EXKF,AQKF
      COMMON/X3/U,V,E,EMKF1,YH1,YH2,YH3,YH4,YK,SQE,A1,AB1,FR0,
     &EPKF1,AD
      CI=CMPLX(0.0,1.0)
      DO 10 I=1,N
      ZK(I)=PKZ(I)*R0*CI
10    T(I)=U(I)*CEXP(ZK(I))+V(I)*CEXP(-ZK(I))
      RETURN
      END
C
      SUBROUTINE RADIAL(C4,C5,R)
      COMPLEX A1,AB1,Q3,Q4,Q5,C4,C5,CLOG,Q6,EPKF1,Q10,Q12
      DIMENSION C4(5),C5(5),YK(25),FR0(5),EPKF1(9),EMKF1(9)
      DIMENSION YH1(9,25),YH2(9,25),YH3(9,25),YH4(9,25),U(9),V(9)
      COMPLEX YH1,YH2,YH3,YH4,YK,U,V,EMKF1,FR0,Q41,Q42,Q7,Q8,Q9
      COMMON/X1/R0,DD,TV
      COMMON/X3/U,V,E,EMKF1,YH1,YH2,YH3,YH4,YK,SQE,A1,AB1,FR0,
     &EPKF1,AD
      PI=3.14159265
      SQP=SQRT(PI)
      Q1=AD/R
      Q2=Q1*Q1
```

```
      Q3=AB1*AB1
      Q11=1./Q1
      Q41=(AB1+Q11)/(AB1-Q11)
      Q42=CLOG(Q41)
      Q4=Q1*Q42
      Q6=-2.*AB1*Q2+Q3*Q2*Q4
      Q5=1./(Q3-Q11*Q11)
      Q7=2.*Q1-AB1*Q1*Q4
      Q8=(Q1*Q2*Q3*Q4*AB1)
      Q9=Q2*Q1*Q3
      Q10=2.*Q3*Q3*Q2*Q2*Q5
      Q12=4.*Q3*AB1*Q2*Q2*Q4
      SQ3=SQRT(3.*PI)
      SQ5=SQRT(5.*PI)
      I=1
      C4(I)=SQP*Q4
      C4(I+1)=SQ3*Q7
      C4(I+2)=SQ5*((3./2.)*Q6-0.5*Q4)
      C4(I+3)=SQRT(7.*PI/4.)*(5.*((2./3.)*Q1+2.*Q9-Q8)-3.*Q7)
      C4(I+4)=35.*((-2./3.)*AB1*Q2-2.*Q3*AB1*Q2*Q2+Q3*Q3*Q2*Q2*Q4
     &)-30.*(-2.*AB1*Q2+Q3*Q4*Q2)+3.*Q4
      C4(I+4)=C4(I+4)*(3./8.)*SQP
      C5(I)=2.*SQP*Q5
      C5(I+1)=SQ3*Q1*(-2.*AB1*Q5+Q4)
      C5(I+2)=SQ5*(3.*Q2-3.*AB1*Q2*Q4+Q5*(3.*Q3*Q2-1))
      C5(I+3)=SQRT(7.*PI/4.)*(5.*(-4.*AB1*Q1*Q2-2.*Q3*AB1*Q2*Q1*Q5+
     &3.*Q3*Q4*Q2*Q1)-3.*C5(I+1)/SQ3)
      C5(I+4)=35.*((2./3)*Q2+6.*Q3*Q2*Q2+Q10-Q12)-
     &30.*(2.*Q2+2.*Q3*Q2*Q5-2.*AB1*Q2*Q4)+6.*Q5
      C5(I+4)=C5(I+4)*(3./8.)*SQP
      RETURN
      END
C
      SUBROUTINE TERM4(T4,LMAX,NINT,N,EPS)
      DIMENSION F1(200),F2(200),F3(200),WP(4,4,4),VP(4,4,4)
      DIMENSION YK(25),U(9),V(9),F(200),FR0(5),PKZ(9),EPKF1(9)
      DIMENSION YH1(9,25),YH2(9,25),YH3(9,25),YH4(9,25)
      DIMENSION D4(5,200),D5(5,200),XP(4,4,4,4),YP(4,4,4,4),F4(200)
      DIMENSION A2(5,200),A3(5,200),E1(5,200),ZP(4,4,4,4),EMKF1(9)
      COMPLEX D4,D5,A2,A3,E1,E2M,EPKF1,E2P,F4
      COMPLEX CI,YK,U,V,Q,P2,F,T4,EXKF,EMKF1,A1,AB1
      COMPLEX EPS,YH1,YH2,YH3,YH4,Y1,Y2,P1,XP,YP,ZP
      COMPLEX F1,F2,F3,R1,FR0,WP,VP,PKZ,BJ1,BJ2,BN1,BN2
      COMMON/X1/R0,DD,TV
      COMMON/X2/AKF,AKP,AQ,ALPHA,PKZ,EXKF,AQKF
      COMMON/X3/U,V,E,EMKF1,YH1,YH2,YH3,YH4,YK,SQE,A1,AB1,FR0,
     &EPKF1,AD
      COMMON/X4/D4,D5,A2,A3,E1
      COMMON/X6/F1,F2,F3,F,XP,YP,ZP,WP,VP
      DATA CI,PI/(0.0,1.0),3.14159265/
      Q=8.*PI*A1*EPS*AQ*EXKF
      Q=Q/(AQKF*(1.-EPS))
      T4=0.0
      AL=0.
      AH=R0
```

```
      M=0
      C=(AH-AL)/(NINT-1)
      DO 20 IG=1,N
      DO 10 IL=1,LMAX+3
      L=IL-1
      CL=FLOAT(L)
      LC=L*(L+1)+M+1
      Y1=YH3(IG,LC)
      Y2=YH4(IG,LC)
      IF((CABS(Y1).EQ.0.).AND.(CABS(Y2).EQ.0.))GOTO 10
      P1=CI**L
      DO 40 K=1,NINT
      IF(K.EQ.1)GOTO 31
      X=AL+(K-1)*C
      E2P=EPKF1(IG)*X
      E2M=EMKF1(IG)*X
      CALL CALXBF(E2P,CL,BJ1,BN1)
      CALL CALXBF(E2M,CL,BJ2,BN2)
      F1(K)=U(iG)*Y1*BJ1
      F2(K)=V(iG)*Y2*BJ2
      F(K)=F1(K)-F2(K)
      F4(K)=F1(k)+F2(K)
      F3(K)=(F(K)*CI*PKZ(IG)*D4(IL,K)-0.5*D5(IL,K)*F4(K)/AD)*X*X
      GO TO 40
 31   F3(K)=0.
 40   CONTINUE
      CALL SINT(AL,AH,F3,NINT,R1)
      P2=R1*P1
      T4=T4+P2
 10   CONTINUE
 20   CONTINUE
      T4=T4*Q
      RETURN
      END
C
      SUBROUTINE ALM(AL1,N,L,M)
      DIMENSION U(9),V(9),YK(25),YH1(9,25),YH2(9,25)
      DIMENSION YH3(9,25),YH4(9,25),FR0(5),EPKF1(9),EMKF1(9)
      COMPLEX A1,AB1,AL1,R,S1,BJ,BN,S,CONJG,FR0,CI,EPKF1
      COMPLEX YK,U,V,EMKF1,YH1,YH2,YH3,YH4,Y1,Y2,Y3,Q
      COMMON/X1/R0,DD,TV
      COMMON/X3/U,V,E,EMKF1,YH1,YH2,YH3,YH4,YK,SQE,A1,AB1,FR0,
     &EPKF1,AD
      DATA CI,PI/(0.0,1.0),3.14159265/
      Q=4.*PI
      S=0.0
      LC=L*(L+1)+M+1
      CL=FLOAT(L)
      S1=SQE*R0
      CALL CALXBF(S1,CL,BJ,BN)
      DO 20 IG=1,N
      Y1=CONJG(YH1(IG,LC))
      Y2=CONJG(YH2(IG,LC))
      IF((CABS(Y1).EQ.0.).AND.(CABS(Y2).EQ.0.))GOTO 20
      Y3=Y1*U(IG)+Y2*V(IG)
```

```
      S=S+Y3*BJ
 20   CONTINUE
      R=(CI**L)*S*Q
      AL1=R/FR0(L+1)
      RETURN
      END
C
      SUBROUTINE TERM6(T6,NINT,LMAX,EPS,N)
      DIMENSION F1(200),F2(200),F3(200),YK(25),F(200)
      DIMENSION FI(200),DFI(200),ATP(200),X(200),PKZ(9)
      DIMENSION U(9),V(9),C4(5),C5(5),XP(4,4,4,4),YP(4,4,4,4)
      DIMENSION YH1(9,25),YH2(9,25),YH3(9,25),YH4(9,25)
      DIMENSION A3(5,200),A2(5,200),E1(5,200),D4(5,200),FR0(5)
      DIMENSION D5(5,200),ZP(4,4,4,4),WP(4,4,4),EPKF1(9)
      DIMENSION XL(4),FJ(4),DFJ(4),VP(4,4,4),EMKF1(9)
      COMPLEX FJ,DFJ,EPKF1,XP,YP,ZP,WP,VP
      COMPLEX A2,A3,E1,D4,D5,R1,C2,Y2,Y1
      COMPLEX YH1,YH2,YH3,YH4,A1,AB1,C4,C5
      COMPLEX FL,DFL1,DFL,DFL3,X1,X2,X3,FIR0,FR0
      COMPLEX YK,FI,DFI,U,V,EPS,EXKF,EMKF1,T6,Q1
      COMPLEX DEL,BJ1,BN1,S1,F,F1,F2,F3,CI,AL1,PKZ
      COMMON/X1/R0,DD,TV
      COMMON/X2/AKF,AKP,AQ,ALPHA,PKZ,EXKF,AQKF
      COMMON/X3/U,V,E,EMKF1,YH1,YH2,YH3,YH4,YK,SQE,A1,AB1,FR0,
     &  EPKF1,AD
      COMMON/X4/D4,D5,A2,A3,E1
      COMMON/X5/X,ATP,Z,CL,EE,NMESH,KRMT,JRKI,NF,INDP,IP
      COMMON/X6/F1,F2,F3,F,XP,YP,ZP,WP,VP
      DATA CI,PI/(0.0,1.0),3.14159265/
      Q1=16.*PI*AQ*A1*EPS*EXKF*PI
      Q1=Q1/((1.-EPS)*AQKF)
      T6=0.0
      JRKI=NF
      EE=E
      AL=0.
      AH=R0
      C=(AH-AL)/(NINT-1)
      LX=LMAX+3
      DO 10 IL=1,LX
      L=IL-1
      CL=FLOAT(L)
      CALL CALXFI(FI,DFI,DEL,E,L,FIR0)
      FR0(IL)=FIR0/R0
      DO 10 K=2,NINT
      XN=AL+(K-1)*C
      IF(L.GT.0)GO TO 25
      CALL RADIAL(C4,C5,XN)
      DO 28 LL=1,5
      D4(LL,K)=C4(LL)
 28   D5(LL,K)=C5(LL)
 25   S1=AKF*XN
      CALL CALXBF(S1,CL,BJ1,BN1)
      E1(IL,K)=BJ1
      FI(K)=FI(K)/XN
      DFI(K)=(DFI(K)-FI(K))/XN
```

```
      DO 60 ITEST=1,200
      IF(X(ITEST).GT.XN)GOTO 61
60    CONTINUE
61    JL=ITEST
      IF(ITEST.LE.2)JL=3
      XL(1)=X(JL-2)
      XL(2)=X(JL-1)
      XL(3)=X(JL)
      XL(4)=X(JL+1)
      FJ(1)=FI(JL-2)
      FJ(2)=FI(JL-1)
      FJ(3)=FI(JL)
      FJ(4)=FI(JL+1)
      DFJ(1)=DFI(JL-2)
      DFJ(2)=DFI(JL-1)
      DFJ(3)=DFI(JL)
      DFJ(4)=DFI(JL+1)
      CALL INTERP(XL,FJ,XN,FL,DFL1)
      CALL INTERP(XL,DFJ,XN,DFL,DFL3)
      A2(IL,K)=FL
      A3(IL,K)=DFL
10    CONTINUE
      LM=LMAX+1
      LM1=LM+1
      DO 12 IL3=1,LM
      L3=IL3-1
      DO 12 IL2=1,LM1
      L2=IL2-1
      DO 14 IL1=1,LM1
      L1=IL1-1
      DO 14 M1=-L1,L1
      IM1=IABS(M1)
      IF(IM1.GT.L3)GOTO 14
      CALL ALM(AL1,N,L3,M1)
      LC=L1*(L1+1)+M1+1
      Y1=YK(LC)
      IF(CABS(Y1).EQ.0.)GOTO 14
      Y2=AL1
      Y2=Y2*Y1
      Y2=Y2*(-CI**L1)
      C1=FLOAT(((2*L1+1)*(2*L2+1)*(2*L3+1)*FAK(L1-IM1)*FAK(L3-IM1))
     &/(FAK(L1+IM1)*FAK(L3+IM1)*4.*PI))
      C1=SQRT(C1)/(4.*PI)
      C2=C1*Y2
      X1=XP(IL3,IL2,IL1,IM1+1)
      X2=YP(IL3,IL2,IL1,IM1+1)
      X3=ZP(IL3,IL2,IL1,IM1+1)
      IF((CABS(X1).EQ.0.).AND.(CABS(X2).EQ.0.).AND.(CABS(X3).EQ.
     &0.))GOTO 14
      DO 15 K=2,NINT
      XN=AL+(K-1)*C
      F1(K)=X1*XN*XN*A3(IL3,K)
      F2(K)=(F1(K)+0.5*X2*A2(IL3,K)*XN)*D4(IL2,K)
      F3(K)=F2(K)-0.5*X3*A2(IL3,K)*D5(IL2,K)*XN*XN/AD
      F(K)=F3(K)*E1(L1+1,K)
```

```
 15   CONTINUE
      CALL SINT(AL,AH,F,NINT,R1)
      T6=T6+R1*C2
 14   CONTINUE
 12   CONTINUE
      T6=T6*Q1
      WRITE(*,108)T6
 108  FORMAT(1X,'T6',2E12.4)
      RETURN
      END
C
      SUBROUTINE TERM9(T9)
      DIMENSION U(9),V(9),YK(25),YH1(9,25),YH2(9,25),YH3(9,25)
      DIMENSION YH4(9,25),FR0(5),PKZ(9),EPKF1(9),EMKF1(9)
      COMPLEX U,V,T9,Q1,EXKF,EMKF1,X1,X2,X3,CI,PKZ
      COMPLEX YK,YH1,YH2,YH3,YH4,A1,AB1,FR0,EPKF1
      COMMON/X1/R0,DD,TV
      COMMON/X2/AKF,AKP,AQ,ALPHA,PKZ,EXKF,AQKF
      COMMON/X3/U,V,E,EMKF1,YH1,YH2,YH3,YH4,YK,SQE,A1,AB1,FR0,
     &EPKF1,AD
      CI=CMPLX(0.0,1.0)
      Q1=4.*AQ*A1*CI*CEXP(CI*AKF*(R0+DD/2))
      Q1=Q1*TV*SQE
      Y1=(SQE-AKF)
      Y2=(SQE+AKF)
      X1=U(1)/Y1
      X1=X1*SIN(Y1*DD/4)
      X2=V(1)/Y2
      X2=X2*SIN(Y2*DD/4)
      X3=X1-X2
      T9=Q1*X3
      WRITE(*,11)T9
 11   FORMAT(1X,'T9',2E12.4)
      RETURN
      END
C
      SUBROUTINE TERM8(T8,N)
      DIMENSION YK(25),U(9),V(9),F(200),YH1(9,25),YH2(9,25),FR0(5)
      DIMENSION YH3(9,25),YH4(9,25),F1(200),F2(200),F3(200)
      DIMENSION A2(5,200),A3(5,200),E1(5,200)
      DIMENSION PKZ(9),D4(5,200),D5(5,200),XP(4,4,4,4),YP(4,4,4,4)
      DIMENSION ZP(4,4,4,4),WP(4,4,4),VP(4,4,4),EPKF1(9),EMKF1(9)
      COMPLEX XP,YP,ZP,WP,VP,PKZ
      COMPLEX A2,A3,E1,FR0,CONJG,EPKF1,D4,D5
      COMPLEX YH1,YH2,YH3,YH4,A1,AB1,F1,F2,F3,Y1,Y2
      COMPLEX CI,YK,U,V,F,Q,EXKF,EMKF1,T8,E2M,E2P
      COMMON/X1/R0,DD,TV
      COMMON/X2/AKF,AKP,AQ,ALPHA,PKZ,EXKF,AQKF
      COMMON/X3/U,V,E,EMKF1,YH1,YH2,YH3,YH4,YK,SQE,A1,AB1,FR0,
     &EPKF1,AD
      COMMON/X4/D4,D5,A2,A3,E1
      COMMON/X6/F1,F2,F3,F,XP,YP,ZP,WP,VP
      DATA CI,PI/(0.0,1.0),3.14159265/
      Q=8.*PI*CI*A1/AQKF
      Q=Q*AQ*2.*SQRT(PI)*CEXP(CI*AKF*(R0+DD/2))
```

```
      T8=0.
      LC=1
      DO 20 IG=1,N
      Y1=CONJG(YH3(IG,LC))
      Y2=CONJG(YH4(IG,LC))
      IF((CABS(Y1).EQ.0.).AND.(CABS(Y2).EQ.0.))GOTO 20
      F1(IG)=CSIN(EPKF1(IG)*R0)/(EPKF1(IG)**3)
      F2(IG)=R0*CCOS(EPKF1(IG)*R0)/(EPKF1(IG)*EPKF1(IG))
      F2(IG)=(F1(IG)-F2(iG))*Y1*U(IG)
      F3(IG)=CSIN(EMKF1(IG)*R0)/(EMKF1(IG)**3)
      F(IG)=R0*CCOS(EMKF1(IG)*R0)/(EMKF1(IG)*EMKF1(IG))
      F(IG)=(F3(IG)-F(IG))*Y2*V(IG)
      T8=T8+PKZ(IG)*(F2(IG)-F(IG))
 20   CONTINUE
      T8=Q*T8
      WRITE(*,22)T8
 22   FORMAT(1X,'T8',2E12.4)
      RETURN
      END
C
      SUBROUTINE TERM10(T10,NINT,LMAX,N)
      DIMENSION F1(200),F2(200),YK(25),F3(200),F(200),XP(4,4,4,4)
      DIMENSION FR0(5),PKZ(9),D4(5,200),YP(4,4,4,4)
      DIMENSION U(9),V(9),YH1(9,25),YH2(9,25),YH3(9,25),YH4(9,25)
      DIMENSION A2(5,200),A3(5,200),E1(5,200),D5(5,200)
      DIMENSION ZP(4,4,4,4),WP(4,4,4),VP(4,4,4),EPKF1(9),EMKF1(9)
      COMPLEX A2,A3,E1,EPKF1,XP,ZP,YP,WP,VP
      COMPLEX YK,EMKF1,U,V,CI,FR0,D4,D5
      COMPLEX EXKF,T10,Q1,R1,F3,Y1,Y2,C2,PKZ
      COMPLEX YH1,YH2,YH3,YH4,A1,AB1,F,F1,F2,AL1,X1,X2
      COMMON/X1/R0,DD,TV
      COMMON/X2/AKF,AKP,AQ,ALPHA,PKZ,EXKF,AQKF
      COMMON/X3/U,V,E,EMKF1,YH1,YH2,YH3,YH4,YK,SQE,A1,AB1,FR0,
     &EPKF1,AD
      COMMON/X4/D4,D5,A2,A3,E1
      COMMON/X6/F1,F2,F3,F,XP,YP,ZP,WP,VP
      DATA CI,PI/(0.0,1.0),3.14159265/
      Q1=16.*AQ*A1*PI
      Q1=Q1*PI*CEXP(CI*AKF*(R0+DD/2))/AQKF
       T10=0.0
       AL=0.
       AH=R0
       C=(AH-AL)/(NINT-1)
       LM=LMAX+1
       DO 10 IL3=1,LM
       L3=IL3-1
       DO 12 IL1=1,LMAX+2
       L1=IL1-1
       DO 12 M1=-L1,L1
       IM1=IABS(M1)
       IF(IM1.GT.L3)GOTO 12
       CALL ALM(AL1,N,L3,M1)
       Y1=AL1
       LC=L1*(L1+1)+M1+1
       Y2=YK(LC)
```

```
      IF(CABS(Y2).EQ.0.)GOTO 12
      Y2=Y1*Y2
      C1=FLOAT(((2*L1+1)*(2*L3+1)*FAK(L3-IM1)*FAK(L1-IM1))/
     &(FAK(L1+IM1)*FAK(L3+IM1)))
      C1=SQRT(C1)/(4.*PI)
      C2=C1*Y2*(-CI**L1)
      X1=WP(IL3,IL1,IM1+1)
      X2=VP(IL3,IL1,IM1+1)
      IF((CABS(X1).EQ.0.).AND.(CABS(X2).EQ.0.))GOTO 12
      DO 15 K=2,NINT
      XN=AL+(K-1)*C
      F1(K)=X1*A3(IL3,K)*XN*XN
      F2(K)=X2*A2(IL3,K)*XN*0.5
      F3(K)=(F1(K)+F2(K))*E1(IL1,K)
15    CONTINUE
      CALL SINT(AL,AH,F3,NINT,R1)
      T10=T10+R1*C2
12    CONTINUE
10    CONTINUE
      T10=T10*Q1
      RETURN
      END
```

APPENDIX IV

```
C       DIPOLE SUM FOR DIAMOND LATTICE-ZERO'TH PLANE
        DOUBLE PRECISION R1,R2,R3,R4,R5,R6,X3,X1,X2,S
        READ (1,*) M,N3
        X3=FLOAT(N3)
        S=0.0
        M1=(M+1)/2
        R3=X3*X3
        DO 10 I=1,M
        N1=I-M1
        X1=FLOAT(N1)
        DO 20 J=1,M
        N2=J-M1
        X2=FLOAT(N2)
        R1=(X1*X1+X2*X2)*0.5+R3
        R2=3.*R3-R1
        R4=DSQRT(R1)
        R5=R4*R4*R4*R4*R4
        R6=R2/R5
        S=(S+R6)
  20    CONTINUE
        WRITE (6,*) N1,S
  10    CONTINUE
        S1=S/8.
        WRITE(6,32) M,N3,S,S1
32      FORMAT(2X,'M',I5,2X,'N3',I1,5X,'S',E16.7,2X,'S1',E16.7)
        STOP
        END
C       DIPOLE SUM FOR THE 1ST PLANE
        DOUBLE PRECISION X,SUM,R1,R2,R3,R4
        REAL N1,N2
        READ (1,*) M,N3
        SUM=0.0
        DO 3 I=1,M
        N1=FLOAT(I-(M+1)/2)
        DO 2 J= 1,M
        N2= FLOAT(J-(M+1)/2)
        R1=N1**2+N2**2+N1*N2
        R2=(8/3)*N3**2
        R3=DSQRT(R1+R2)
        R4=R3*R3*R3*R3*R3
        X=(2*R2-R1)/R4
        SUM=SUM+X
  2     CONTINUE
        WRITE (1,*) SUM,X
  3     CONTINUE
        WRITE (1,10) M,SUM,N3
 10     FORMAT (2X,'M=',I4,10X,'SUM=',E14.5,8X,'N3=',I2)
        STOP
        END
C       DIPOLE SUM FOR DIAMOND LATTICE-2ND PLANE
        DOUBLE PRECISION R1,R2,R3,R4,R5,R6,R7,RO,X1,X2,X3
        READ(1,*)M,N3
        X3=FLOAT(N3)
```

```
      S=0.0
      M1=(M+1)/2
      RO=FLOAT(M1)
      R3=(X3+0.5)*(X3+0.5)
      DO 10 I=1,M
      N1=I-M1
      X1=FLOAT(N1)
      DO 20 J=1,M
      N2=J-M1
      X2=FLOAT(N2)
      R1=(X1+0.5)*(X1+0.5)*(0.5)
      R2=R1+(X2+0.5)*(X2+0.5)*(0.5)
      R4=R2+R3
      R5=DSQRT(R4)
      IF(R5.GT.RO) GO TO 20
      R6=R5*R5*R5*R5*R5
      R7=(3.*R3-R4)/R6
      S=S+R7
   20 CONTINUE
      IF(I/20.EQ.I/20) WRITE(6,31) N1,S
   10 CONTINUE
      S=S/8.
      WRITE(6,32) M,N3,S
   31 FORMAT(2X,'N1=',I5,2X,'S FOR N1=',E16.7)
   32 FORMAT(2X,'M=',I5,2X,'N3=',I1,5X,'SUM=',E16.7)
      STOP
      END

C     DIPOLE SUM FOR DIAMOND LATTICE-3RD PLANE
      DOUBLE PRECISION R1,R2,R3,R4,R5,R6,R7,RO,X1,X2,X3
      READ(1,*)M,N3
      X3=FLOAT(N3)
      S=0.0
      M1=(M+1)/2
      RO=FLOAT(M1)
      R3=(X3+0.75)*(X3+0.75)
      DO 10 I=1,M
      N1=I-M1
      X1=FLOAT(N1)
      DO 20 J=1,M
      N2=J-M1
      X2=FLOAT(N2)
      R1=(X1+0.5)*(X1+0.5)*(0.5)
      R2=R1+(X2+1)*(X2+1)*0.5
      R4=R2+R3
      R5=DSQRT(R4)
      IF(R5.GT.RO) GO TO 20
      R6=R5*R5*R5*R5*R5
      R7=(3.*R3-R4)/R6
      S=S+R7
   20 CONTINUE
      IF(I/20.EQ.I/20) WRITE(6,31) N1,S
   10 CONTINUE
      WRITE(6,32) M,N3,S
   31 FORMAT(2X,'N1=',I5,2X,'S FOR N1=',E16.7)
```

```
 32   FORMAT(2X,'M=',I5,2X,'N3=',I1,5X,'SUM=',E16.7)
      STOP
      END
C
C     MAIN PROGRAM TO CALCULATE  DIPOLE FIELD AND DIPOLE MOMENT
C     DENSITY
      DIMENSION A(33,33),P(33),X(33),E(33),INT(33)
      EMACH=1.0E-06
      PB=-3.14159*8./3.
      READ(1,*) NMAX,IT,GS,DG
      NR=NMAX
      NC=NMAX
      AZ=-3.193856
      A1=-2.086166
      A2=-0.505366
      A3=-0.00618
      A4=0.0080
      WRITE(6,100) AZ,A1,A2,A3,A4
100   FORMAT(8E12.4)
      DO 999 N=1,IT
      DO 10 I=1,NMAX
      DO 10 J=1,NMAX
10    A(I,J)=0.0
      G=GS+DG*(N-1)
      GZ=-AZ*G
      G1=-A1*G
      G2=-A2*g
      G3=-A3*G
      G4=-A4*G
      WRITE(6,101) G
101   FORMAT (2X,'GAMA=',F7.4)
      DO 20 I=1,NMAX
      X(I)=1.0
      E(I)=0.0
      P(I)=0.0
20    A(I,I)=1.0+GZ
      DO 30 I=1,NMAX
      IF(I-4.EQ.0) GO TO 22
      A(I,I-4)=G4
      A(I-4,I)=G4
 22   CONTINUE
      IF(I-3.LE.0) GO TO 31
      A(I,I-3)=G3
      A(I-3,I)=G3
31    CONTINUE
      IF(I-2.LE.0) GO TO 32
      A(I,I-2)=G2
      A(I-2,I)=G2
32    CONTINUE
      IF(I-1.LE.0) GO TO 33
      A(I,I-1)=G1
      A(I-1,I)=G1
33    CONTINUE
30    CONTINUE
      DO 5 I=1,7
```

```
5       WRITE(6,109) (A(I,J),J=1,7)
109     FORMAT(2X,7E10.3)
        CALL ZGE(A,INT,NR,NC,EMACH)
        CALL ZSU(A,INT,X,NR,NC,EMACH)
        NB=(NMAX+1)/2
        C=X(NB)
        DO 38 I=1,NB
38      WRITE(6,102) I,X(I)
102     FORMAT(2X,'I=',I2,2X,'X(I)=',F8.4)
        DO 40 I=1,NMAX
40      X(I)=X(I)/C
        DO 50 I=1,NB
        P(I)=AZ*X(I)+A1*X(I+1)+A2*X(I+2)+A3*X(I+3)+A4*X(I+4)
        IF(I.GT.1) P(I)=P(I)+A1*X(I-1)
        IF(I.GT.2) P(I)=P(I)+A2*X(I-2)
        IF(I.GT.3) P(I)=P(I)+A3*X(I-3)
        IF(I.GT.4) P(I)=P(I)+A4*X(I-4)
50      E(I)=P(I)/PB
        CC=P(NB)
        DO 60 I=1,NB
        P(I)=P(I)/CC
60      WRITE(6,103) I,X(I),P(I),E(I)
103     FORMAT(2X,'I=',I2,2X,'X=',F16.4,2X,'P=',F16.4,2X,'E=',F16.4)
999     CONTINUE
        STOP
        END
```

INDEX

Modern Physics Letters B, Vol. 5, No. 1 (1991) 65–72

PHOTOEMISSION CALCULATION WITH A SIMPLE MODEL FOR THE PHOTON FIELD: APPLICATION TO ALUMINIUM

P. DAS, R. K. THAPA* AND N. KAR
Department of Physics, University of North Bengal, Siliguri, West Bengal 734 430 India

Received 26 September 1990

Photoemission cross-sections are calculated, using a simple "local" dielectric function for computing the photon field in the surface region and free electron wavefunctions. Comparisons are made with the experimental data for the frequency-dependent normal photoemission from the Fermi level of aluminium, and the importance of the variation of the photon field in the surface region is pointed out.

1. Introduction

Photoemission experiments on surfaces of solids are basically concerned with the excitation of electrons by the incident photon energy. A simple calculation of photo-current (in one-electron approximation) involves the evaluation of matrix elements of the form $\langle\psi_i|H'|\psi_f\rangle$, where $|\psi_i\rangle$ and $|\psi_f\rangle$ denote the initial and final one-electron states whose energies are connected by $E_f - E_i = \hbar\omega$ and $H' = (e/2mc).(\mathbf{p}.\mathbf{A} + \mathbf{A}.\mathbf{p})$, $\mathbf{p}$ being the one-electron momentum operator and $\mathbf{A}$, the vector potential associated with the photon field. The states $|\psi_i\rangle$ and $|\psi_f\rangle$ are modified from the bulk-states by the presence of the surface. Similarly, the photon field also has a spatial variation in the surface region.

In standard photoemission calculations,[1,2] the one-electron states are calculated with a high degree of accuracy — but the variation of the photon field is generally neglected. Depending on the type of experimental data one intends to compare the calculation with, this may or may not be a reasonable approximation. In the case where one looks at the photoemission current as a function of photon energy with a constant initial state, the photon field variation in the surface region needs to be considered more carefully. However, a first principles calculation of the electromagnetic field in the presence of a surface is an extremely complex problem — only for the case of jellium the results are available.[3,4] Bagchi and Kar, on the other hand, computed the field in a simple "local" model, using experimentally determined frequency-dependent dielectric

PACS No.: 79.60
*Present address: Department of Physics, Pachhunga University College, Aizawl, Mizoram 796001, India

functions as parameter, and they used this for calculation of photo-current from the surface state of tungsten.[5] This simple model is applicable to those elements for which the frequency-dependent dielectric functions are known. In this paper, we use this model in conjunction with free-electron wavefunctions for electron states and show that the results obtained agree qualitatively with experimental data and the theoretical results obtained by more sophisticated jellium field calculations. This would indicate that we may use the simple model for calculation of photoemission cross-sections of other metals for which the jellium results would not be applicable.

2. Formalism

The golden-rule expression for the current density[6] may be written as

$$\frac{di(E)}{d\Omega} = \frac{2\pi}{\hbar} \sum |\langle \psi_f | H' | \psi_i \rangle|^2 \delta(E - E_f)\, \delta(E_f - E_i - \hbar\omega) f_0(E - \hbar\omega)[1 - f_0(E)] \,, \tag{1}$$

where H' is the perturbation responsible for photoemission by radiation of frequency ω, $|\psi_i\rangle$ and E_i refer to the initial state wavefunction and energy and $|\psi_f\rangle$ and E_f to the final state wavefunction and energy, and $f_0(E)$ denotes the Fermi occupation function. We are considering the photoemission to take place along z-axis, which is normal to the surface. We may therefore write H' as

$$H' = (e/mc)\left[\tilde{A}_\omega(z)\frac{d}{dz} + \frac{1}{2}\frac{d}{dz}\tilde{A}_\omega(z)\right], \tag{2}$$

where $\tilde{A}_\omega(z) = \dfrac{A_\omega{}^z(z)}{A_0}$ with $A_\omega{}^z(z)$ as the component of vector potential along z-axis, and A_0 is the amplitude of the incident beam. The formula for photoemission cross-section can be written as

$$\frac{d\sigma}{d\Omega} \approx \frac{k^2}{\omega} |\langle \psi_f | \tilde{A}_\omega(z) \frac{d}{dz} + \frac{1}{2}\frac{d}{dz}\tilde{A}_\omega(z) | \psi_i \rangle|^2 \,. \tag{3}$$

The model of Bagchi and Kar is employed for the computation of $\tilde{A}_\omega(z)$. We assume the z-direction to be perpendicular to the nominal surface which is chosen as $z = 0$. The metal is assumed to occupy all space to the left of the $z = 0$ plane. The response of the electromagnetic field is bulk-like everywhere except in the surface region defined by $-a \leq z \leq 0$. In this region the model dielectric function is chosen to be a local one which interpolates linearly between the bulk value inside the metal and the vacuum value (unity) outside. The model frequency-dependent dielectric function is therefore given by

$$\varepsilon(\omega) \equiv \varepsilon_1(\omega) + i\varepsilon_2(\omega) \qquad \text{for } z < -a \,,$$

$$\varepsilon(\omega, z) = 1 + [1 - \varepsilon(\omega)]z/a \quad \text{for} \quad -a \leq z \leq 0 \ ,$$
$$1 \quad \text{for} \quad z > 0 \ . \tag{4}$$

For the complex dielectric function $\varepsilon(\omega, z)$ we use the experimental values given by Weaver.[7] We consider p-polarized light to be incident on the surface plane making an angle θ_i with z-axis. The calculated vector potential of interest, $\tilde{A}_\omega(z)$, in the long-wavelength limit $(\omega a/c) \to 0$ is

$$\tilde{A}_\omega(z) = \begin{cases} -\dfrac{\sin 2\theta_i}{[\varepsilon(\omega) - \sin^2\theta_i]^{1/2} + \varepsilon(\omega)\cos\theta_i} \ , & z < -a \\ -\dfrac{\sin 2\theta_i}{[\varepsilon(\omega) - \sin^2\theta_i]^{1/2} + \varepsilon(\omega)\cos\theta_i} \dfrac{a\,\varepsilon(\omega)}{[1 - \varepsilon(\omega)]z + a} \ , & -a \leq z \leq 0 \\ -\dfrac{\varepsilon(\omega)\sin 2\theta_i}{[\varepsilon(\omega) - \sin^2\theta_i]^{1/2} + \varepsilon(\omega)\cos\theta_i} \ , & z > 0 \ . \end{cases} \tag{5}$$

This expression is to be used in the evaluation of the matrix element.

To evaluate the photoemission cross-section we also need the initial and final state wavefunctions. These are calculated in the free electron model with the potential given by

$$V(z) = V_0\theta(z) \ , \tag{6}$$

where $V_0 = E_F + \phi$, E_F being the Fermi level in the free electron model and ϕ the work function, $\theta(z)$ is the step function, $\theta(z) = 0$ for $z < 0$ and $\theta(z) = 1$ for $z > 0$ (see Fig. 1). By matching the wavefunctions at the surface plane $z = 0$, we may write the initial state wavefunction as

$$\psi_i(r) = \begin{cases} (m/2\pi\hbar^2 k_i)^{1/2} \dfrac{1}{L}\left[e^{ik_i z} + \dfrac{ik_i + \kappa}{ik_i - \kappa} e^{-ik_i z}\right] e^{i\mathbf{k}_\parallel \cdot \mathbf{r}_\parallel} \ , & z < 0 \\ (m/2\pi\hbar^2 k_i)^{1/2} \dfrac{1}{L} \dfrac{2ik_i}{ik_i - \kappa} e^{-\kappa z} e^{i\mathbf{k}_\parallel \cdot \mathbf{r}_\parallel} \ , & z > 0 \ , \end{cases} \tag{7}$$

where $k_i^2 = \dfrac{2m}{\hbar^2} E_i - \mathbf{k}_\parallel^2$, $\kappa^2 = \dfrac{2m}{\hbar^2}(V_0 - E_i) + \mathbf{k}_\parallel^2$, and $\mathbf{k}_\parallel$ and $\mathbf{r}_\parallel$ are the components of $\mathbf{k}$ and $\mathbf{r}$ in the κ-y plane (plane parallel to the surface).

Similarly, the final state wavefunction may be written as

$$\psi_f = \begin{cases} (m/2\pi\hbar^2 q)^{1/2} \dfrac{1}{L} \dfrac{2q}{q + k_f} e^{ik_f z} e^{i\mathbf{k}_\parallel \cdot \mathbf{r}_\parallel} \ , & z < 0 \\ (m/2\pi\hbar^2 q)^{1/2} \dfrac{1}{L}\left[e^{iqz} + \left(\dfrac{q - k_f}{q + k_f}\right) e^{-iqz}\right] e^{i\mathbf{k}_\parallel \cdot \mathbf{r}_\parallel} \ , & z > 0 \end{cases} \tag{8}$$

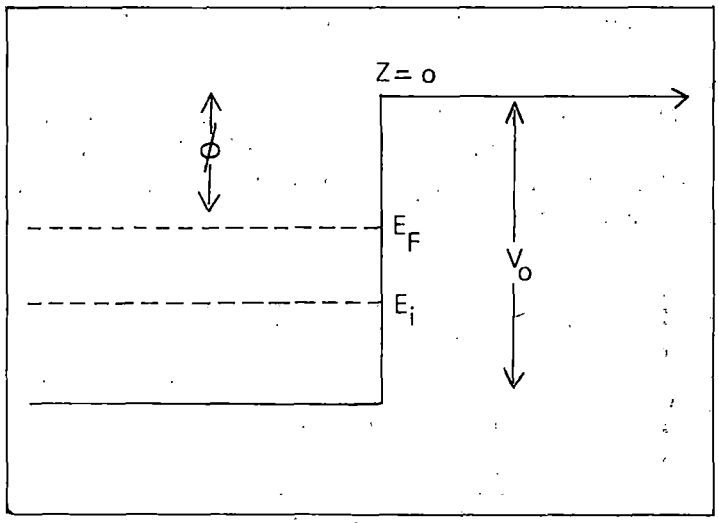

Fig. 1. Model potential used for calculating wavefunctions for initial and final states, $\phi = 4.25$ eV & $V_0 = 15.95$ eV.

where $k_f^2 = \frac{2mE_f}{\hbar^2} - \mathbf{k}_\parallel^2$, $q^2 = \frac{2m}{\hbar^2}(E_f - V_0) - \mathbf{k}_\parallel^2$, $E_f = E_i + \hbar\omega$. The matrix element for photoemission can be evaluated by using the above expressions for the vector potential and the wavefunctions. However, to ensure convergence for $z < 0$, one has to introduce a convergence factor due to lifetime effects. This is a standard procedure in low energy electron diffraction and photoemission calculations (see, for example, Pendry[2]). We do it here by introducing a factor $e^{-\alpha|z|}$ (for $z < 0$) in the calculation of the matrix element – this is to take into account the inelastic scattering of electrons.

3. Application

We have applied our results for computing the normal photoemission from the Fermi level of Aluminium, for which experimental results as well as theoretical calculations using jellium model are available. The experimental results are shown in Fig. 2, the data of Levinson *et al.*[8] having been used. For our calculations, we have taken $\phi = 4.25$ eV and $E_F = 16.7$ eV — these values have been given by Ashcroft and Mermin.[9] Since normal photoemission is considered, $\mathbf{k}_\parallel = 0$; also θ_i is taken to be 45° as in the experiment. Our results for the photoemission cross-section are shown in Fig. 3 (with $a = 10$ atomic units). We see that there is qualitative agreement between the experimental data and calculated photo-currents. The calculated curve shows a peak at 11 eV, a

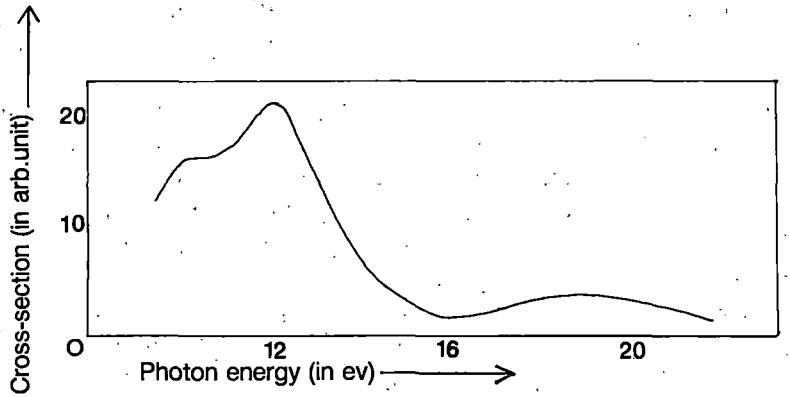

Fig. 2. Experimental data of photoemission cross-section for aluminium for normal emission from Fermi level, (100) face, as a function of photon energy (from Levinson *et al.*[8]).

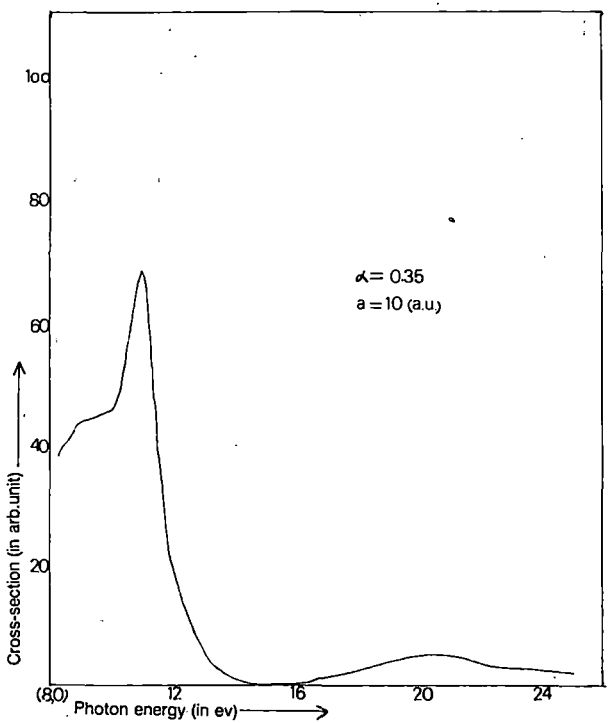

Fig. 3. Calculated photoemission cross-section from Fermi level of aluminium as a function of photon energy.

minimum at 15 eV and again a broad peak around 20.5 eV. These features are also present in the experimental curve — although the shapes of the two curves are different.

We further investigated the origin of the peak at 11 eV in the calculated spectrum and concluded that it is a surface feature. As evidence for that we plot the field $|\tilde{A}_\omega(z)|$ as a function of z in the surface region for $\hbar\omega = 11$ eV (Fig. 4). We see that there is a strong peak in the middle of the surface region. For $\hbar\omega = 15$ eV and 20 eV, on the other hand (Fig. 4), the plot of $|\tilde{A}_\omega(z)|$ does not show any peak in the surface region.

As further evidence of the peak at 11 eV being surface-related, we show the results of a calculation of photo-current with fields given by the Fresnel refraction formulae at the surface, i.e., the fields are given by

$$\tilde{A}_\omega(z) = \begin{cases} -\dfrac{\sin 2\theta_i}{[\varepsilon(\omega) - \sin^2\theta_i]^{1/2} + \varepsilon(\omega)\cos\theta_i}, & z < 0 \\ -\dfrac{\varepsilon(\omega)\sin 2\theta_i}{[\varepsilon(\omega) - \sin^2\theta_i]^{1/2} + \varepsilon(\omega)\cos\theta_i}, & z > 0\,, \end{cases} \tag{9}$$

and the (free-electron) wavefunctions are the same as in Eqs. (7) and (8). We see that, although there is a minimum around 12 eV, there is no peak around

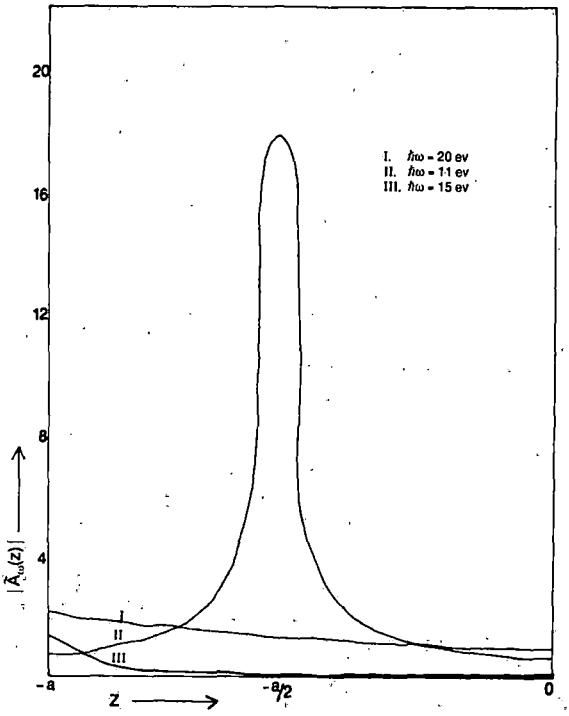

Fig. 4. Plot of $|\tilde{A}_\omega(z)|$ vs. z in the surface region for $\hbar\omega = 11$ eV, 15 eV and 20 eV.

11–12 eV (Fig. 5). Above the plasmon frequency, the curve shows a peak which is much more pronounced than that in the calculation with a surface region. The peak in the experimental data above the plasmon frequency is also much less pronounced. Anyway, it is quite clear that the calculations with the simple Fresnel refraction formulae is not even qualitatively correct – in particular it completely fails to reproduce the peak around 11–12 eV.

We have thus shown that with a simple local model for the dielectric function, we can get a qualitative agreement with experimental data. There have been previous calculations, notably by Levinson *et al.*[8] and Barberan and Inglesfield[10] for aluminium. The calculations of Levinson *et al.*, employing the self-consistent jellium model for fields in the surface region are more sophisticated and their results are in better agreement with the experimental data. However, the calculations for jellium cannot be extended to more complicated cases, e.g., transition metals or semiconductors, while the model we have employed can be extended to these cases. So the qualitative agreement we obtain in aluminium and the previous application to the case of tungsten gives us confidence to apply our model to photoemission calculations for other metals and semiconductors. However, for these cases, we cannot use free electron wavefunctions any more.

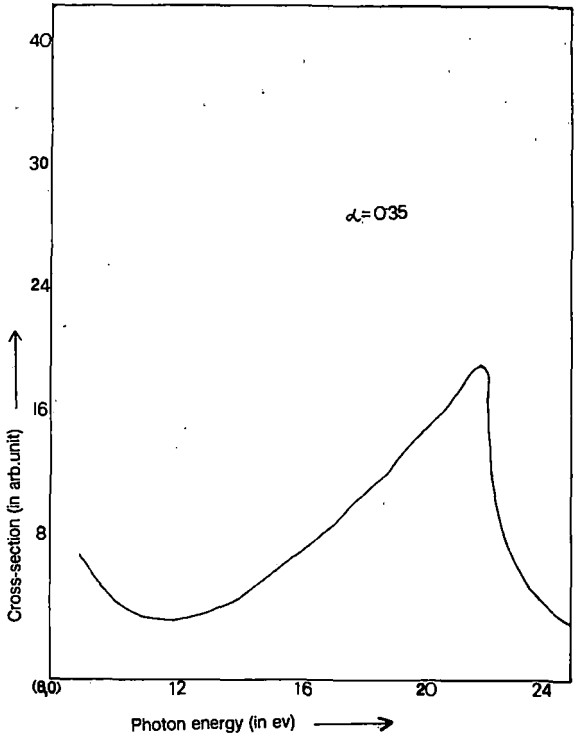

Fig. 5. Photoemission cross-section from Fermi level of aluminium with Fresnel fields.

We are working to combine a better description of the wavefunction with the field given by this model for photo-current calculations of other metals.

In conclusion, although there are shortcomings in the model for electromagnetic field employed here (for example, since experimentally measured dielectric functions are used as inputs, the origin of the surface-related peak cannot be exactly pin-pointed) — it gives results in reasonable agreement with experimental data, and has the potential of being used for a number of metals and semiconductors.

Acknowledgement

One of the authors (N. K.) acknowledges a grant from Council of Scientific and Industrial Research, India.

References

1. A. Liebsch, *Phys, Rev. Lett.* **32** (1974) 1203.
2. J. B. Pendry, *Surf. Sci.* **57** (1976) 679; see also J. B. Pendry in *Photoemission and the Electronic Properties of Surfaces*, eds, B. Feurbacher, B. Fitton and R. F. Willis (Wiley, NY, 1978).
3. P. J. Feibelman, *Phys. Rev. Lett.* **34** (1975) 1092; *Phys. Rev.* **B12** (1979) 1319.
4. G. Mukhopadhayay and S. Lundquist, *Solid State Commun.* **21** (1977) 629.
5. A. Bagchi and N. Kar, *Phys. Rev.* **B18** (1978) 5240.
6. D. R. Penn, *Phys. Rev. Lett.* **28** (1972) 1041.
7. J. Weaver in *Handbook of Chemistry and Physics of Solids* (CRC Press Boca Raton, Ohio, 1987) E-377.
8. H. J. Levinson, E. W. Plummer and P. J. Feibelman, *Phys. Rev. Lett.* **43** (1979) 953 and *J. Vac. Sci. Technol.* **17** (1980) 216.
9. N. W. Ashcroft and N. D. Mermin, *Solid State Physics*, (Holt, Reinhart and Winston, NY, 1976) p. 38.
10. N. Barberan and J. E. Inglesfield, *J. Phys.* **C14** (1981) 3114.

phys. stat. sol. (b) **187**, 551 (1995)

Subject classification: 71.10 and 79.60; S4

Department of Physics, North Bengal University, Siliguri[1])

Photoemission Calculations Including Both Band Structure Effects and Photon Field Variation

By

P. DAS and N. KAR

Photoemission cross-sections are calculated, using band wave functions and a spatially varying photon field. The solid is considered to be composed of a stack of identical layers of atoms parallel to the surface with a potential of muffin-tin form. The photoemission matrix element is calculated by appropriate expansion of the initial and final state wave function and the vector potential of the photon field in the muffin-tin, interstitial, and vacuum regions. The case of normal photoemission from the (100) face of aluminium is considered as an application.

1. Introduction

Experimental data from angle-resolved photoemission measurements have been very useful in surface physics, and to analyze the data, methods for photoemission calculation [1, 2] have been developed where the wave functions for the semi-infinite solid are constructed accurately. However, the variation of the photon field is generally neglected in such calculations. An accurate calculation of the electromagnetic field in the surface region is itself a complex problem and first principles calculations are available [3, 4] only for jellium. It has not been possible so far to construct a theory of photoemission incorporating both LEED-type wave functions and RPA-type field calculation. In any case, transition metals and semiconductors would be beyond the purview of such calculations.

On the other hand, empirical calculations of fields near surfaces with 'local' dielectric function have been used to explain certain qualitative features of photoemission data for tungsten [5], palladium [6], and aluminium [7]. Even with simplistic wave functions, using the measured energy-dependent dielectric function, this approach has been reasonably successful.

This work is an improvement on our previous photocurrent calculations [7] using free electron states. Here we have included the crystal potential in muffin-tin form to calculate the initial state wave function. The formalism has been applied to the case of normal photoemission of electrons at the Fermi level from the (100) face of aluminium and the results have been compared with experimental data as well as previous calculations.

2. Scheme of Calculations

The photoemission cross-section can be written, in the Golden Rule approximation [8], as

$$\frac{\mathrm{d}j(E)}{\mathrm{d}\Omega} = \frac{2\pi}{\hbar} \sum_{\mathrm{f,i}} |\langle \psi_\mathrm{f}| H' |\psi_\mathrm{i}\rangle|^2 \, \delta(E - E_\mathrm{f}) \, \delta(E_\mathrm{f} - E_\mathrm{i} - \hbar\omega) \, f_0(E - \hbar\omega) \, [1 - f_0(E)] \,, \tag{1}$$

[1]) Siliguri 734430, West Bengal, India.

where ψ_i and ψ_f are the initial and final states and $H' = (e/2mc)(\boldsymbol{A}\cdot\boldsymbol{p} + \boldsymbol{p}\cdot\boldsymbol{A})$, $\boldsymbol{A}$ being the vector potential of the photon field and $\boldsymbol{p}$ the one-electron momentum operator. To evaluate the matrix element we have to construct ψ_f and ψ_i and to determine $\boldsymbol{A}$.

We shall assume the solid to be composed of a stack of identical layers of atoms parallel to the surface. Further, within each layer there is one atom per unit cell and the centres of all the atoms lie in the same plane parallel to the surface. We consider the crystal potential to be of muffin-tin form. This description is the same as that for many standard photoemission calculations, e.g. Pendry [2, 9], and we may use the same form for the wave function in each layer.

2.1 Initial and final state wave functions

For each layer, we expand the wave functions in spherical harmonics inside the muffin-tin sphere and in the interstitial regions, since the potential is constant, the wave functions can be expanded into forward and backward travelling plane waves. For the vacuum region, the initial state wave function can be constructed by considering a wave function decaying exponentially outside the surface. With the centre of the muffin-tin sphere in the layer chosen as the origin, the initial state wave function may be written as

$$\psi_i(\boldsymbol{r}) = \begin{cases} \sum_L Z_L f_1(R)\, Y_L(\theta,\varphi)\,; & \text{spherical region}\,, \\ \sum_g [u_g\, e^{iK_g^+\cdot R} + v_g\, e^{iK_g^-\cdot R}]\,; & \text{interstitial region}\,, \\ \sum_g T_g\, e^{iK_g\cdot(r-r_0)_\parallel}\, e^{-\chi_g(z-z_0)}\,; & \text{vacuum region}\,, \end{cases} \tag{2}$$

where

$$\boldsymbol{K}_g^{\pm} = [(\boldsymbol{k}+\boldsymbol{g})_\parallel, \pm\sqrt{2(E_i - V_0) - |\boldsymbol{k}+\boldsymbol{g}|_\parallel^2}]\,,$$

$$\chi_g = \sqrt{-[2E_i - (\boldsymbol{k}+\boldsymbol{g})_\parallel^2]}\,, \quad \text{and} \quad \boldsymbol{R} = \boldsymbol{r} - \boldsymbol{c}_j\,,$$

with $\boldsymbol{g}$ denoting two-dimensional reciprocal lattice vectors and $\boldsymbol{K}_g^{\pm}$ the wave vector of the emitted electrons. $\boldsymbol{c}_j$ is the origin at the j-th layer and V_0 the constant interstitial potential with respect to vacuum. u_g, v_g are determined by LEED-type band structure calculations. Z_L, T_g etc. are determined by matching at the appropriate surface. Here $z = z_0$ is the surface plane with respect to the origin in the first layer.

The final state wave function may also be determined as in LEED calculations, but for computational simplicity we have taken it to be in free electron form. Since we want to apply this method to cases where the principal effect is due to the spatial variation in the photon field, we expect this approximation not to affect our results qualitatively. We may write the final states as [7]

$$\psi_f(\boldsymbol{r}) = \begin{cases} e^{i\boldsymbol{q}\cdot(\boldsymbol{r}-\boldsymbol{r}_0)} + \dfrac{q - k_f}{q + k_f}\, e^{-i\boldsymbol{q}\cdot(\boldsymbol{r}-\boldsymbol{r}_0)}\,; & z > z_0\,, \\ \dfrac{2q}{q + k_f}\, e^{i\boldsymbol{k}_f\cdot(\boldsymbol{r}-\boldsymbol{r}_0)}\,; & z < z_0\,, \end{cases} \tag{3}$$

where

$$k_f^2 = \frac{2mE_f}{\hbar^2} - k_\parallel^2\,, \qquad q^2 = \frac{2m}{\hbar^2}(E_f - V_0) - k_\parallel^2\,, \qquad E_f = E_i + \hbar\omega\,.$$

2.2 *Photon field*

To compute the photon field we use the simple model given by Bagchi and Kar [5] where the metal is assumed to occupy all the space to the left of the surface plane $z = z_0$ and the extent of the surface region is $-a \leqq z \leqq z_0$. We may write the expression for the photon field for the p-polarized light in the long-wavelength limit as

$$A(z) = \begin{cases} A_1\,; & \text{bulk region}\,, \\ \dfrac{A_1\varepsilon(\omega)/[1-\varepsilon(\omega)]}{\dfrac{z}{a}+\beta}\,; & \text{surface region}\,, \\ A_1\varepsilon(\omega)\,; & \text{vacuum region}\,, \end{cases} \tag{4}$$

where A_1 and β are constants, depending on the dielectric function ε, the photon energy $\hbar\omega$, and the angle of incidence θ. We have taken the surface region to be the same as the first layer, otherwise the evaluation of the matrix element becomes too cumbersome. We may also consider the surface layer to be equal to an integral number of layers. Although we are using this form for the vector potential, any vector potential which is a function only of the coordinate normal to the surface may be used.

2.3 *Matrix element*

We may write down the matrix element (in (1)) for the solid as a whole,

$$\langle\psi_\mathrm{f}|\,H'\,|\psi_\mathrm{i}\rangle = \int_{\text{vac.}} \psi_\mathrm{f}^* H'\psi_\mathrm{i}\,\mathrm{d}^3r + \int_{\text{surf.}} \psi_\mathrm{f}^* H'\psi_\mathrm{i}\,\mathrm{d}^3r + \sum_j \int_{\text{bulk}} \psi_\mathrm{f}^* H'\psi_\mathrm{i}\,\mathrm{d}^3r\,, \tag{5}$$

where in each region the wave functions and the vector potentials corresponding to that region have to be used. For the vacuum region the integration can be performed analytically with the appropriate forms for ψ_i, ψ_f, and A. Inside each layer, the integration has to be performed over both the spherical and the interstitial regions.

The evaluations of the integral over the interstitial region is somewhat more complicated because of the shape of the region. To do it, we perform the integration over the whole layer, using the form ψ_i for the interstitial region, then subtract the contribution from the muffin-tin sphere.

The integration over the whole layer is simple and comes out as a one-dimensional integration given by

$$T_1 = p_1 S_0 \int_{z_1}^{z_0} \left[\frac{iK_{gz}^+}{\dfrac{z}{a}+\beta} \{u_0\,\mathrm{e}^{iK_{gfz}^+ z} - v_0\,\mathrm{e}^{iK_{gfz}^- z}\} - \frac{1}{2a\left(\dfrac{z}{a}+\beta\right)^2} \{u_0\,\mathrm{e}^{iK_{gfz}^+ z} + v_0\,\mathrm{e}^{iK_{gfz}^- z}\} \right] \mathrm{d}z\,, \tag{6}$$

where

$$p_1 = \frac{2qA_1\varepsilon\,\mathrm{e}^{i\boldsymbol{k}_\mathrm{f}\cdot\boldsymbol{r}_0}}{(q+k_\mathrm{f})(1-\varepsilon)} \quad \text{and} \quad \boldsymbol{K}_{gf}^{\pm} = \boldsymbol{K}_g^{\pm} - \boldsymbol{k}_\mathrm{f}\,,$$

where S_0 is the area of the surface unit cell and z_1 the layer boundary between the first and second layers.

For evaluating the integral over the muffin-tin sphere, we have to expand wave functions and the z-component of the vector potential spherically. For ψ_i or ψ_f we use the following standard expansion:

$$e^{iK_g^{\pm}\cdot r} = 4\pi \sum_L i^l j_l(|K_g^{\pm}|\, r)\, Y_{lm}(r)\, Y_{lm}^*(K_g^{\pm})\,. \tag{7}$$

To express A_z in spherical coordinates, we write it in the following form:

$$A_z(z) = A_z(r\cos\theta) = \frac{1}{\dfrac{r}{a}\cos\theta + \beta} = \sum_l B_l(r)\, P_l(\cos\theta) \tag{8}$$

with

$$B_l(r) = \frac{2}{2l+1}\int_0^{\pi} A_z(r\cos\theta)\, P_1(\cos\theta)\sin\theta\, d\theta\,.$$

We have calculated the coefficient $B_l(r)$ analytically using standard integration tables [10]. The values of $B_l(r)$ for $l = 0$ and $l = 1$ are given by

$$B_0(r) = \frac{2a}{r}\ln\left[\frac{\dfrac{r}{a}+\beta}{-\dfrac{r}{a}+\beta}\right], \qquad B_1(r) = \frac{2}{3}\left[\frac{2a}{r} - \beta\left(\frac{a}{r}\right)^2 \frac{\dfrac{r}{a}+\beta}{-\dfrac{r}{a}+\beta}\right]. \tag{9}$$

The terms involving A_z' may also be evaluated similarly in terms of $D_l(r)$.

We calculate the matrix element in the muffin-tin region using the interstitial wave functions for the initial state. This term may be written as

$$T_2 = 8\pi p_1 \sum_{g,l} \frac{i^l}{2l+1} \times \left[\left\{iK_{gz}^{+}\int_0^{r_m}\left[u_g P_l(K_p^{+})\, j_l(|K_{gf}^{+}|\, r) - v_g P_l(K_p^{-})\, j_l(|K_{gf}^{-}|\, r)\right] B_l(r)\, r^2\, dr\right\} - \left\{\frac{1}{2a}\int_0^{r_m}\left[u_g P_l(K_p^{+})\, j_l(|K_{gf}^{+}|\, r) + v_g P_l(K_p^{-})\, j_l(|K_{gf}^{-}|\, r)\right] D_l(r)\, r^2\, dr\right\}\right], \tag{10}$$

where $K_p^{\pm} = K_{gf}^{\pm}\cdot\hat{z}$ and r_m is the muffin-tin radius.

Using the radial wave functions for the initial state inside the muffin-tin sphere we calculate the integration as a product of a radial part, which has to be evaluated numerically and another one involving the Clebsch-Gordan coefficients. The integral may be written as

$$T_3 = 8\pi p_1 \sum_{L_1,l_2,L_3} \frac{Z_{L_3}(-i)^{l_1}\, Y_{L_1}(k_f)}{2l_2+1}\int_0^{r_m}\left[\left\{C_{L_1 l_2 L_3}^{1}\left[\frac{\partial}{\partial r} f_{L_3}(r)\right] r^2 + C_{L_1 l_2 L_3}^{2} f_{l_3}(r)\, r\right\} \times B_{l_2}(r) - \frac{1}{2a}\, C_{L_1 l_2 L_3}^{3} f_{l_3}(r)\, r^2 D_{l_2}(r)\right] j_{l_1}(k_f r)\, dr\,, \tag{11}$$

where C_l are the Clebsch-Gordan coefficients. Therefore, the surface layer contribution to the matrix element can be obtained from the relation $T_s = T_1 - T_2 + T_3$.

For the bulk layers the matrix element can similarly be calculated for the muffin-tin and interstitial regions but since the photon field is a constant here, integrations are simpler compared to that for the surface layer. Almost all of these integrations have to be performed numerically.

3. Application

We have applied this method to normal photoemission from the Fermi level of aluminium as a function of photon energy. The muffin-tin potential and the crystal parameters used are those given by Pendry [9]. For the band structure calculation the imaginary part of the crystal potential has been taken to be zero.

For the photon field calculation, the data given by Weaver [11] for the complex dielectric function of aluminium as a function of photon energy were used. Since the final state was taken to be free electron like, a convergence factor of exp $(-\alpha z)$ was introduced in the final state. We have taken [12] $E_f = 11.7$ eV, $V_0 = 15.95$ eV, and the lattice constant for aluminium as 0.405 nm. In Fig. 1 we show the result [13] obtained for normal photoemission ($k_{\|} = 0$) for a p-polarized photon incident at 45° to the surface normal. The two curves shown correspond to two different values for the parameter a defining the surface region in the field calculation (4). The curve with open circles is for a taken to be the same as the thickness of the first layer while the plot with filled circles is for a equal to the thickness of the first two layers. We note here that we have taken the first layer width to be different from the other layers — this was done so that the surface plane can be taken to be tangential to the last layer of muffin-tins. The scales of photocurrent for the two curves are not the same, we have plotted them so that the peaks around 11 eV are of comparable height. The value of α was taken to be 0.35 (the same value used earlier with free electron initial and final states).

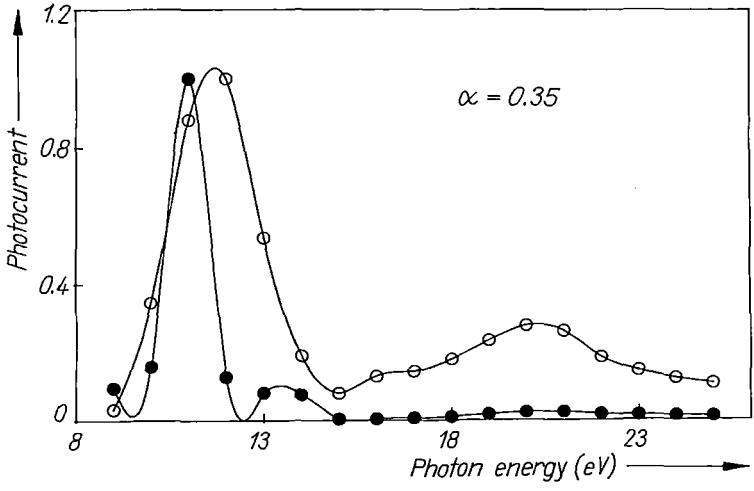

Fig. 1. Variation of the photocurrent (arb. units) with photon energy for normal photoemission from the Fermi level of the aluminium (100) face with the surface region a for field variation. Open circles for a taken equal to the thickness of the first layer, full circles for a equal to the thickness of the first two layers

The calculated photocurrent shows a peak at 11.5 eV followed by a minimum at the plasmon energy ($\approx$16 eV) and a broad maximum around 20 eV. We have seen that these features are also present in the experimentally observed results [14, 15] and in our previously calculated [7] photocurrents. In the experimental curve for the photocurrent, we have seen that the ratio of the peak heights of the two peaks (below and above the plasmon energy) is of the order of 6 and in our previous result it was 15 but now this ratio comes out to be $\approx$3.6 for a equal to the thickness of the first layer only and $\approx$23 for a equal to the thickness of the first two layers.

So, we may conclude that use of band wave functions gives better agreement compared to previous calculations with free electron wave functions. From Fig. 1 it is evident that the field variation may be taken to be over the first layer only, at least with this model. For a complete calculation of photocurrent we have included LEED-type final states and work for that is in progress part of which has already been reported.

Acknowledgements

Some of the subroutines and the muffin-tin potential for aluminium have been taken from the book Low Energy Electron Diffraction written by Pendry [9]. One of the authors (P. D.) thanks CSIR, India for a research fellowship and the other author (N. K.) thanks CSIR for a research grant.

References

[1] A. LIEBSCH, Phys. Rev. Letters **32**, 1203 (1974).
[2] J. B. PENDRY, Surface Sci. **57**, 679 (1976); Photoemission and the Electronic Properties of Surfaces, Ed. B. FEURBACHER, B. FITTON, and R. F. WILLIS, Wiley, New York 1978.
[3] P. J. FEIBELMAN, Phys. Rev. Letters **34**, 1092 (1975); Phys. Rev. B **12**, 1319 (1975).
[4] G. MUKHOPADHYAY and S. LUNDQUIST, Solid State Commun. **21**, 629 (1977).
[5] A. BAGCHI and N. KAR, Phys. Rev. B **18**, 5240 (1978).
[6] R. K. THAPA, phys. stat. sol. (b) **179**, 391 (1993).
[7] P. DAS, R. K. THAPA, and N. KAR, Mod. Phys. Letters B **5**, 65 (1991).
[8] D. R. PENN, Phys. Rev. Letters **28**, 1041 (1972).
[9] J. B. PENDRY, Low Energy Electron Diffraction, Academic Press, London 1974.
[10] I. S. GRADSHTEYN and I. M. RYZHIK, Tables of Integrals, Academic Press, London/New York 1980.
[11] J. WEAVER, Handbook of Chemistry and Physics of Solids, CRC Press, Inc., Boca Raton (Ohio) 1978 (E-377).
[12] N. W. ASHCROFT and N. D. MERMIN, Solid State Physics, Holt, Reinehart, and Winston Publ., New York 1976 (p. 38).
[13] P. DAS, DAE SSP Symp. '93, **46**, 36C (1993).
[14] H. J. LEVINSON, E. W. PLUMMER, and P. J. FEIBELMAN, Phys. Rev. Letters **43**, 953 (1979); J. Vacuum Sci. Technol. **17**, 216 (1980).
[15] N. BARBERAN and J. E. INGLESFIELD, J. Phys. C **14**, 3114 (1981).

(Received June 24, 1994)

Modern Physics Letters B, Vol. 6, No. 20 (1992) 1263–1272

DIPOLAR FIELDS NEAR THE SURFACE FOR CRYSTALS WITH SIMPLE HEXAGONAL, HEXAGONAL CLOSE-PACKED AND DIAMOND STRUCTURE

P. DAS and N. KAR
Physics Department, North Bengal University, Siliguri, West Bengal 734 430, India

Received 7 July 1992

The dipolar local field near the surface for simple hexagonal, hexagonal close-packed and diamond structure has been computed by considering a slab geometry. The technique of plane by plane summation for dipolar fields has been used and self-consistent field determined with large enough number of layers.

The local, or effective electric field for a polarizable infinite lattice has been studied for a long time (see for example, Born and Wolf[1]). The self-consistent local electric field near the surface of a dipolar lattice for simple cubic, face-centred and body centred cubic structures have also been calculated.[2] In this paper, we consider three other structures, simple hexagonal, hexagonal close-packed (hcp) and diamond structure. The first two do not belong to the cubic system and so the Lorentz–Lorenz relation is not expected to hold (although, for the "ideal" hcp structure, the relation does hold); the Bravais lattice for the diamond structure is face-centred cubic, but the fact that there exists a two-atom basis means that in addition to the atomic sites for the face-centred cubic structure there would be an equal number of atoms in other sites and the local field in the surface plane is quite different from the face-centred cubic case, as we shall discuss later.

The procedure for calculating the self-consistent local field is essentially the same as in Ref. 2; we have also used similar notations. A slab geometry of finite number of lattice plane have been considered — the lattice planes are assumed to be infinite, parallel to the surface. We have considered an electric field normal to the surface plane; the polarizability tensor was assumed to be diagonal; the molecules in each site would be polarized — these were taken as point dipoles — and all the dipoles lying in one plane would be parallel to one another and would have the same magnitude. The first step is to compute the field from an infinite two-dimensional lattice of parallel dipoles of equal moment. This can be evaluated either by explicit sum within a finite region and approximating the rest by an integration

PACS No.: 78.20.

with uniform dipole density[3] or by transforming the discrete lattice sum to a highly convergent sum analytically.[4–6] We have used the former technique to evaluate the two-dimensional lattice sum.

Let us denote different planes by the index ν and take $\mathbf{P}_\nu$ to be the local dipole moment density for the lattice plane ν. We shall consider $\nu = 0$ to be the reference plane—positive values of ν denote planes with a positive value of z (above the reference plane) and negative ν values refer to planes below the reference plane. We shall consider an applied field $\mathbf{E}_0 = E_0 \hat{z}$ in the z-direction. The field from the dipoles in the plane ν will depend linearly on P_ν and the z-component of the total contribution of all the dipole fields may be written as

$$E_{d,z} = \sum\nolimits_\nu \xi_\nu P_\nu \,, \tag{1}$$

where the sum over ν includes in principle all the planes in the slab we are considering and the coefficient ξ_ν has to be determined for each lattice structure. However, only a few of the ξ_ν's have non-zero values—at least to the accuracy we are concerned with. We shall give expressions for evaluating ξ_ν for each of the structures we consider.

We now consider a slab of L lattice planes. The local electric field at a lattice point in the μth plane, ($\mu = 1, 2, \ldots L$) may be written as

$$E^\mu_{\mathrm{loc},z} = E_0 + \sum\nolimits_\nu \xi_{\mu-\nu} P_\nu \,, \tag{2}$$

where the sum over ν is from 1 to L (although, in practice, only those terms for which ξ's are non-zero have to be retained).

Taking the volume polarizability to be Γ, the self-consistency condition for the local dipole moment density, given below:

$$P_\mu = \Gamma E^\mu_{\mathrm{loc},z} \tag{3}$$

will yield the matrix equation

$$\sum\nolimits_\nu M_{\mu\nu} P_\nu = \Gamma E_0 \,, \quad \mu = 1, 2, \ldots L \tag{4}$$

where

$$M_{\mu\nu} = [(1 - \Gamma\xi_0)\delta_{\mu\nu} - \Gamma\xi_{\mu-\nu}(1 - \delta_{\mu\nu})] \,. \tag{5}$$

Inversion of the matrix M, where it is permissible, gives us the self-consistent dipole moment density on each plane; in particular, it would give the behaviour near the surface. Then, by using formula (2) we can compute the dipolar field on each plane.

In the following we shall consider the three structures—simple hexagonal, hexagonal close-packed and diamond, separately. In each case we shall give expressions for ξ and compute the self-consistent dipole moment and the dipolar field plane by plane. We shall also discuss the significance of the results obtained.

1. Simple Hexagonal Structure

For the simple hexagonal lattice, the sites in a plane with reference to an origin at a lattice point may be written as

$$\mathbf{R} = a\left[\left(n_1 + \frac{n_2}{2}\right)\hat{x} + \frac{\sqrt{3}}{2}\, n_2 \hat{y}\right] \tag{6}$$

and for any other plane parallel to it, we may write

$$\mathbf{E} = a\left[\left(n_1 + \frac{n_2}{2}\right)\hat{x} + \frac{\sqrt{3}}{2}\, n_2 \hat{y} + \alpha n_3 \hat{z}\right] \tag{7}$$

where $\alpha = c/a$ and the surface is taken to be perpendicular to the z-axis. The electric field due to a dipole of moment $\mathbf{d}_i$ at point $\mathbf{r}_i$ is

$$\mathbf{E}_\mathbf{d} = \sum_i{}' \frac{3(\mathbf{d}_i - \mathbf{r}_i) - r_i^2 \mathbf{d}_i}{r_i^j}\,. \tag{8}$$

If we consider $\mathbf{r}^j$ as the lattice vectors in the reference plane (given by (6)) and noting that if $\mathbf{d}\mu$ is the dipole moment for the dipole in the plane μ, then the dipole moment density for that plane is

$$\mathbf{P} = \frac{2\mathbf{d}_\mu}{\sqrt{3}\,\alpha a^3}\,. \tag{9}$$

We can write the expression for ξ_0 as

$$\xi_0 = -\left(\frac{\sqrt{3}}{2}\,\alpha\right) \sum_{n_1, n_2}{}' \frac{1}{[n_1^2 + n_2^2 + n_1 n_2]^{\frac{3}{2}}} \tag{10}$$

(the point $n_1 = n_2 = 0$ is excluded).

For the other planes, we note that $\xi\mu = \xi - \mu$ and

$$\xi_\mu = \left(\frac{\sqrt{3}}{2}\,\alpha\right) \sum_{n_1, n_2} \frac{3n_3^2\alpha^2 - [n_1^2 + n_2^2 + n_1 n_2 + \alpha^2 n_3^2]}{[n_1^2 + n_2^2 + n_1 n_2 + \alpha^2 n_3^2]^{\frac{5}{2}}} \tag{11}$$

with the plane index $\mu = n_3$. The values of ξ_0, ξ_1, etc. calculated from (10) and (11) are shown in Table 1 for $\alpha = 1.59$ (this value is typical of simple hexagonal structures). These are in agreement with the previously computed values.[4,6] Further, to the accuracy we are interested in, it is necessary to take only ξ_0 and ξ_1 into account, so the sum in (2) would be restricted to $|\mu - \nu| \leq 1$.

We have also calculated P_μ/P_b and E_μ/E_b (where P_b and E_b are the bulk values of the dipole moment and the dipole field) for a 21-layer film with a number of values

Table 1. ξ_μ for various planes for simple hexagonal, hexagonal close-packed and diamond structure.

Plane Index	ξ_μ			
	Hexagonal	Hexagonal close-packed		Diamond
μ	$\alpha = 1.59$	$\alpha = 1.63$	$= 1.86$	
0	−15.6046	−7.8023	−7.8023	−3.1939
1	0.0043	−0.2868	−0.1460	−2.0862
2	0.0000	0.0015	0.0003	−0.5054
3	0.0000	0.0006	0.0000	−0.0062
4	0.0000	0.0000	0.0000	0.0080
5	0.0000	0.0000	0.0000	0.0000

of Γ. (We have seen that 21 layers are enough to ensure convergence; actually, in this case convergence may be achieved even with a fewer number of layers). Except for a very small range near $\Gamma = -0.064$ for which the matrix cannot be inverted, the results look the same—with virtually no change at the surface plane for the dipole moment or the dipolar field. This is not unexpected, since we have seen that $|\xi_0/\xi_1| \sim 3.6 \times 10^3$, almost the entire contribution to the dipolar field comes from the in-plane dipoles, and so there is almost no variation in P_μ/P_b or E_μ/E_b from plane to plane. In Fig. 1, we have plotted E_μ/E_b and P_μ/P_b for $\Gamma = 0.1$, but there is virtually no change if we take any other value of Γ.

3. Hexagonal Close-Packed Structure

For this structure, in addition to the lattice planes for the simple hexagonal case, we have another set of planes halfway between the former ones. The coefficient ξ_0 can be calculated using the same formula (10) as in the case of simple hexagonal structure, with an additional factor of 1/2 which comes in as there are now two atoms per unit cell. The original planes of the simple hexagonal lattice now become even numbered planes, and we may use (11) to calculate ξ_μ, with an additional factor of 1/2 with $\mu = 2n_3$. For the odd-numbered planes we note that the sites may be denoted by the vectors

$$\mathbf{R} = \left(n_1 + \frac{1}{3}\right)\mathbf{a}_1 + \left(n_2 + \frac{1}{3}\right)\mathbf{a}_2 + \left(n_3 + \frac{1}{2}\right)\mathbf{a}_3$$

$$\text{with } \mathbf{a}_1 = a\hat{x}\,, \quad \mathbf{a}_2 = \frac{1}{2}\,a\hat{x} + \frac{\sqrt{3}}{2}\,a\hat{y}\,, \quad \mathbf{a}_3 = c\hat{z}\,.$$

We can then write, for odd planes

$$\xi_\mu = \frac{\sqrt{3}}{4}\,\alpha \sum_{n_1, n_2} \frac{3\alpha^2\left(n_3 + \frac{1}{2}\right)^2 - \left[\left(n_1 + \frac{n_2}{2} + \frac{1}{2}\right)^2 + \frac{3}{4}\left(n_2 + \frac{1}{3}\right)^2 + \alpha^2\left(n_3 + \frac{1}{2}\right)^2\right]}{\left[\left(n_1 + \frac{n_2}{2} + \frac{1}{2}\right)^2 + \frac{3}{4}\left(n_2 + \frac{1}{3}\right)^2 + \alpha^2\left(n_3 + \frac{1}{2}\right)^2\right]^{\frac{5}{2}}} \tag{12}$$

with $\mu = 2n_3 + 1$.

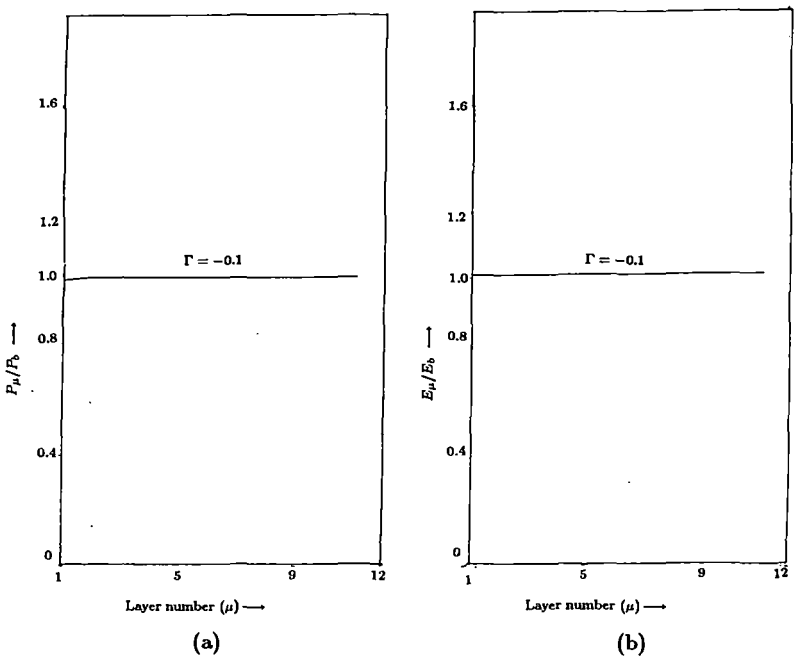

Fig. 1. (a) Variation of dipole moment density, normalized to the uniform bulk value, (P_μ/P_b) against μ, the plane index, for the volume polarizability $\Gamma = -0.1$ in simple hexagonal lattice. (b) Variation of the local dipolar field normalized to its bulk value, (E_μ/E_b) against $\Gamma = -0.1$ in simple hexagonal lattice.

In Table 1, we have shown the computed values of ξ_μ obtained from Eqs. (10), (11) and (12) for two values of α, 1.63 (corresponding to "IDEAL" HCP structure) and 1.86. For cubic symmetry, it is known that

$$\sum\nolimits_\mu \xi_\mu = -\frac{8\pi}{3} \tag{13}$$

which gives the familiar Lorentz–Lorenz result. We note that for the "ideal" HCP structure also, this relation holds, although the symmetry is not cubic. For $\mu = 1.86$ however, the sum over ξ_μ does not give $-8\pi/3$. This is perhaps another illustration of the close relationship between the face-centred cubic and "ideal" hexagonal close-packed structure.

For determining the dipole moment and the dipolar field in the surface region, we have taken a 21 layer slab and constructed the matrix M in (4) and inverted it to obtain the dipole moments P_μ and the dipolar field, layer by layer. It may be mentioned here that taking 21 layer ensures convergence and increasing the number of layers does not change P_μ/P_b or E_μ/E_b, at least to the accuracy we are interested in. For $\alpha = 1.63$, in Fig. 2, we show P_μ/P_b and E_μ/E_b for three values of Γ. Actually the points for integral values of μ are relevant — these points have been joined by lines for visual aid. $\Gamma = -0.10$ and $\Gamma = -0.14$ correspond to

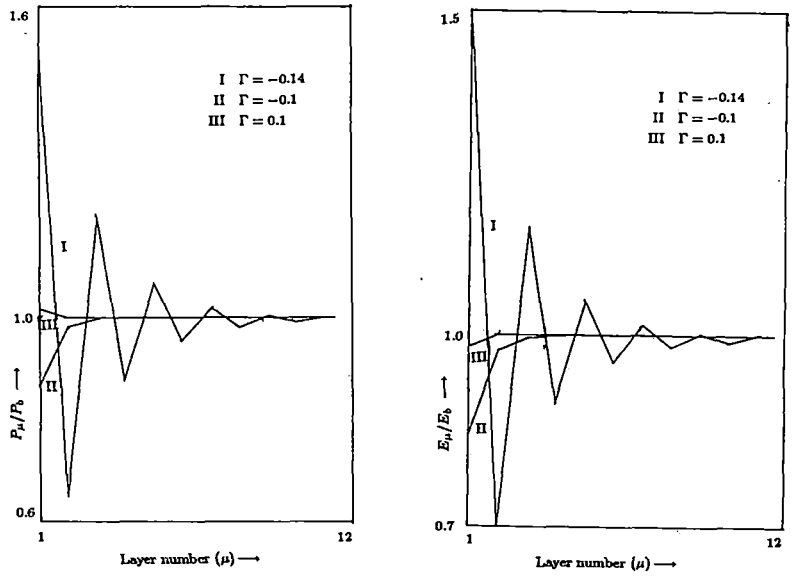

Fig. 2. (a) Variation of P_μ/P_b against μ, the plane index, for $\Gamma = -0.14$, -0.1 and 0.1 in "ideal" hexagonal close-packed structure. (b) Variation of E_μ/E_b against μ, for $\Gamma = -0.14$, -0.1 and 0.1 in "ideal" hexagonal close-packed structure.

values of Γ just beyond the range for which the matrix M may not be inverted. For $\Gamma = -0.14$, i.e., just below the forbidden range, we see the maximum enhancement in the dipolar field for the surface layer, although the enhancement is not very large. The behaviour for both E_μ/E_b and P_μ/P_b is both oscillatory for this value of Γ, again the similarity of behaviour with face-centred cubic case[2] may be noted. For $\Gamma = -0.10$, just above the forbidden range and $\Gamma = 0.1$, the variation in the dipolar field for the surface layer is smaller and the oscillatory behaviour is also absent. For $\alpha = 1.86$, we have plotted P_μ/P_b and E_μ/E_b for the same three values of Γ, and the behaviour is qualitatively the same, but the difference between the surface and bulk values for P_μ (or P_μ) is smaller than for the "ideal" case.

4. Diamond Structure

The diamond structure has the face-centred cubic lattice as the underlying Bravais lattice with a two-atom basis. In this case we have, therefore, in addition to FCC lattice planes, an equal number of planes interspaced between these. For the reference plane, ξ_0 is given by:

$$\xi_0 = -\frac{1}{8}\sum{}'_{n_1,n_2} \frac{1}{\left[\frac{1}{2}(n_1^2+n_2^2)\right]^{\frac{3}{2}}}. \tag{14}$$

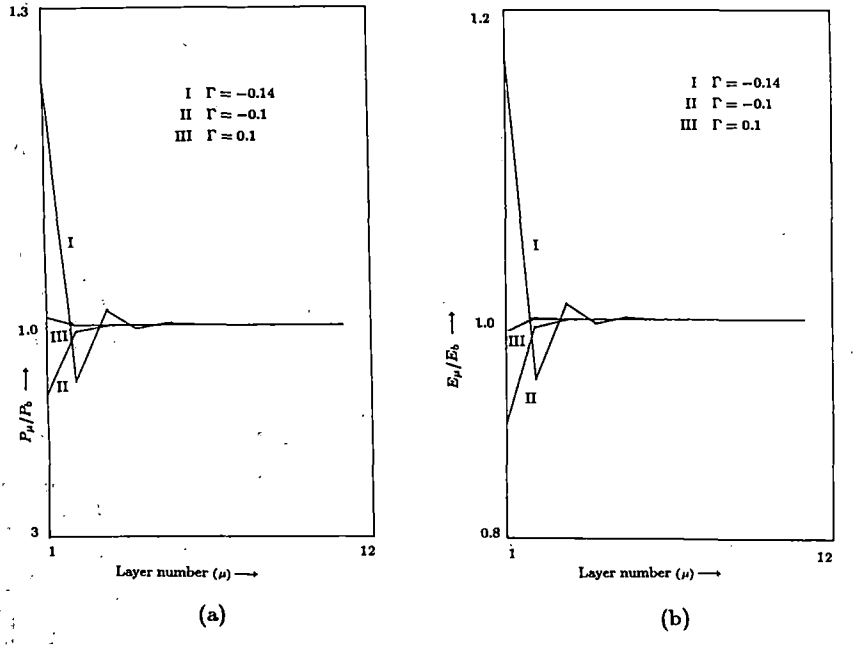

Fig. 3. (a) Variation of P_μ/P_b against μ, for $\Gamma = -0.14$, -0.1 and 0.1 in hexagonal close-packed structure with $\alpha = 1.86$. (b) Variation of E_μ/E_b against μ, for $\Gamma = -0.14$, -0.1 and 0.1 in hexagonal close-packed structure with $\alpha = 1.86$.

For planes located at distance $(n + 1/4)a$ from the reference plane (i.e., 1st plane, 5th plane etc.) we have

$$\xi_\mu = \frac{1}{8} \sum_{n_1,n_2} \frac{3\left(n_3 + \frac{1}{4}\right)^2 - \left[\frac{n_1^2}{2} + \frac{1}{2}\left(n_2 + \frac{1}{2}\right)^2 + \left(n_3 + \frac{1}{4}\right)^2\right]}{\left[\frac{n_1^2}{2} + \frac{1}{2}\left(n_2 + \frac{1}{2}\right)^2 + \left(n_3 + \frac{1}{4}\right)^2\right]^{\frac{5}{2}}} \tag{15}$$

$$\text{with } \mu = 4n_3 + 1 \quad (n_3 = 0, \pm 1, \pm 2, \ldots).$$

For planes at distance $(n + 1/2)a$ from the reference plane (i.e., 2nd, 6th etc.)

$$\xi_\mu = \frac{1}{8} \sum_{n_1,n_2} \frac{3\left(n_3 + \frac{1}{2}\right)^2 - \left[\frac{1}{2}\left(n_1 + \frac{1}{2}\right)^2 + \frac{1}{2}\left(n_2 + \frac{1}{2}\right)^2 + \left(n_3 + \frac{1}{2}\right)^2\right]}{\left[\frac{1}{2}\left(n_1 + \frac{1}{2}\right)^2 + \frac{1}{2}\left(n_2 + \frac{1}{2}\right)^2 + \left(n_3 + \frac{1}{2}\right)^2\right]^{\frac{5}{2}}} \tag{16}$$

$$\text{with } \mu = 4n_3 + 2 \quad (n_3 = 0, \pm 1, \pm 2, \ldots).$$

Similarly, for planes denoted by $\mu = 3, 7, \ldots$ etc.,

$$\xi_\mu = \frac{1}{8} \sum_{n_1,n_2} \frac{3\left(n_3 + \frac{3}{4}\right)^2 - \left[\frac{1}{2}\left(n_1 + \frac{1}{2}\right)^2 + \frac{1}{2}\left(n_2 + 1\right)^2 + \left(\frac{3}{4} + n_3\right)^2\right]}{\left[\frac{1}{2}\left(n_1 + \frac{1}{2}\right)^2 + \frac{1}{2}\left(n_2 + 1\right)^2 + \left(\frac{3}{4} + n_3\right)^2\right]^{\frac{5}{2}}} \tag{17}$$

$$\text{with } \mu = 4n_3 + 3 \quad (n_3 = 0, \pm 1, \pm 2, \ldots)$$

and for planes denoted by $\mu = 4, 8, \ldots$ etc.,

$$\xi_\mu = \frac{1}{8} \sum_{n_1,n_2} \frac{3n_3^2 - \left[\frac{1}{2}(n_1^2 + n_2^2) + n_3^2\right]}{\left[\frac{1}{2}(n_1^2 + n_2^2) + n_3^2\right]^{\frac{5}{2}}} \qquad (18)$$

$$\text{with } \mu = 4n_3 \quad (n_3 = \pm 1, \pm 2, \ldots).$$

The even numbered planes are those in common with the FCC structure—the odd numbered planes are the new ones. As in the previous cases, here also $\xi_\mu = \xi - \mu$; we give the values of ξ_μ in Table 1. Again to the accuracy we are interested, only ξ_0, ξ_1, ξ_2, ξ_3, and ξ_4 (calculated from 14–18) have non-zero values—the rest of them can be taken to be zero. We note also that $\Sigma_\mu \xi_\mu = -8 \cdot \pi/3$ (to 0.05 percent) as is to be expected, since diamond structure has cubic symmetry.

To determine the local field near the surface, we consider for this case a 33 layer slab, we take a larger number of layers as now there are more non-zero ξ_μ's and also because, in contrast to the other cases, the influence of the other two planes above and below the reference plane is comparable to the reference plane itself.

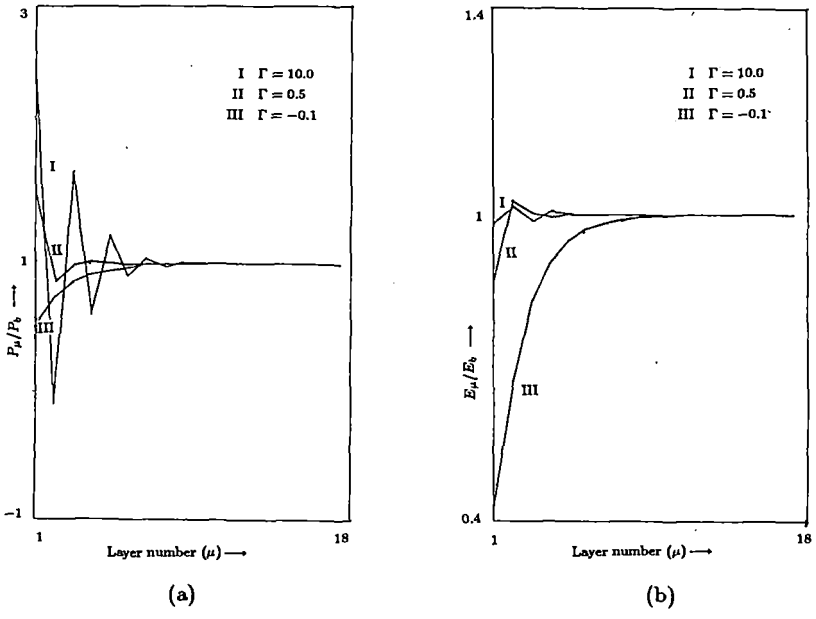

Fig. 4. (a) Variation of P_μ/P_b against μ, the plane index, for $\Gamma = 0.5$, 10.0 and -0.1 in diamond structure. (b) Variation of E_μ/E_b against μ for $\Gamma = 0.5$, 10.0 and 0.1 in diamond structure.

The results for the dipole moment density and the dipolar field obtained by inverting the matrix M also show (Fig. 4) some interesting results. There is a large range of Γ, from $-0.12(\sim -3/8\pi)$ to very large negative values, for which

the inversion process breaks down. We have shown the results for $\Gamma = -0.1$ just above this range. We see the behaviour similar to the other cases—both P_μ/P_b and E_μ/E_b are less than one on the surface plane and monotonically goes to one as we go into the bulk. For large positive values of Γ, $P_{\ddot{\mu}}/P_b$ and $E_{\ddot{\mu}}/E_b$ behave in a different manner. We show in Fig. (4), the results for $\Gamma = 10$. We see that P_μ/P_b has a large oscillatory behaviour. The first layer has a P_μ greater than twice the bulk value, while the second layer has a negative value, i.e., the dipole moment is in the direction opposite that of the bulk! The dipolar field is also oscillatory, but the dipolar fields for the first and second layers are $0.98E_b$ and $1.01E_b$, which is quite a contrast to the behaviour for the dipole moments. This can happen because as we have remarked above, the influence of the two neighbouring planes together is actually greater than that of the reference plane. The oscillations in P_μ are such that their total effect is to make the dipolar field for each layer remains almost the same. For $\Gamma = 0.5$, the results shown in Fig. 4, are similar, but now the oscillations in P_μ/P_b are smaller. For values of Γ larger than 10, the oscillations grow larger and at some stage 33 layers are inadequate to achieve convergence. However, for the values of Γ shown in the Fig. 4 convergence was achieved with 33 layers.

The results for diamond structure are therefore, the most interesting ones. First, there is a large range of Γ for which our procedure breaks down, i.e., for these values of Γ the system can support spontaneous polarization modes. Second, for positive Γ values, we see large changes in dipole moment from layer to layer, but the dipolar field shows much smaller variation. We think that this behaviour can be traced to the fact $|\xi_1| \sim |\xi_0|$, in particular $|2\xi_1/\xi_0| > 1$, which again has its origin in the fact this interlayer spacing $(a/4)$ is smaller than the distance of the in-plane nearest neighbour $(a/\sqrt{2})$.

We have here considered three structures for which the self-consistent dipole moment density and the dipolar fields have been determined layer by layer. From a comparison of these results along with those for the simple cubic, face-centred cubic and body-centred cubic systems, we are led to believe that for the structures (and for the crystallographic directions) for which the interplanar spacing becomes much smaller compared to the distance of the nearest neighbour in the plane, the behaviour of the dipole moment and the local field would be more interesting. However, in no case we have seen an enhancement in the dipolar field for the surface by an order of magnitude or more. This is consistent with the conclusions reached with the cubic structures.

Acknowledgment

One of the authors (N.K.) acknowledges a research grant from C.S.I.R., India, towards this work.

References

1. M. Born and E. Wolf, *Principles of Optics* (Pergamon Press, 1970), Sec. 2.3.
2. N. Kar and A. Bagchi, *Solid State Commun.* **33**, 645 (1980).
3. See, for example, R. Shuttleworth, *Proc. Phys. Soc. (London)* **A62**, 167 (1949).
4. B. R. A. Nijboer and F. W. de Wette, *Physica* **24**, 422 (1958).
5. G. D. Mahan, *J. Chem. Phys.* **43**, 1569 (1965).
6. F. W. De Wette, *Phys. Rev.* **123**, 103 (1961).

Modern Physics Letters B, Vol. 8, No. 6 (1994) 361–366

PHOTOEMISSION CALCULATION WITH KRONIG–PENNEY MODEL

R. K. THAPA
Department of Physics, Pachhunga University College, Aizawl, Mizoram 796 001, India

P. DAS and N. KAR
Department of Physics, North Bengal University, Siliguri, West Bengal 734 430, India

Received 8 July 1993

Photoemission calculations have been performed using the Kronig–Penney model and including photon field variation with the help of a simple model, where the dielectric response in the surface region is a local function linearly interpolated between the vacuum value and the experimentally measured bulk value. Results with different dielectric functions are also presented.

For photoemission calculations, the current density may be written with the help of golden rule expression[1] as

$$\frac{dj(E)}{d\Omega} = \frac{2\pi}{\hbar} \Sigma |\langle \psi_f | H' | \psi_i \rangle|^2 \delta(E - E_f) \delta(E_f - E_i - \hbar\omega) f_0(E - \hbar\omega)[1 - f_0(E)], \quad (1)$$

where $|\psi_i\rangle$ and $|\psi_f\rangle$ refer to the initial and final states, and $H' = (e/2mc)(\mathbf{A}\cdot\mathbf{p} + \mathbf{p}\cdot\mathbf{A})$ with $\mathbf{p}$ being the one electron momentum operator and $\mathbf{A}$ is the vector potential for the photon field. Although the one electron states are treated quite accurately in many photoemission calculations (see, for example, Ref. 2), the variation of the photon field in the surface region is usually neglected. We have used a simple model for field calculations[3] with the experimentally determined photon energy-dependent dielectric functions as the input parameters, and used this in conjunction with free electron wave functions to explain the normal photoemission from the Fermi level for aluminum (100) surface with some success.[4] To incorporate band structure effects, we shall consider here the Kronig–Penney model for the electron states, and determine the photoemission cross section with this model.

The Kronig–Penney model has been used in connection with surface electronic states by several authors.[5,6] It has been seen that some surface related features come out, at least qualitatively, from these calculations. Schaich and Ashcroft[7] have

PACS No.: 79.60-i.

calculated numerically the photo yield by using the modified form of the Kronig–Penney model. Band structure effects were also included in it. They used the wave function of Mitchell[8] for free electron gas in a semi-infinite box and considered the photon field vector to remain constant. However, the numerical data as obtained by them in the case of potassium is quite realistic. This is evident for the nature of the photocurrent data obtained by them from various planes below the surface. Steslicka[9] had performed a detailed calculation of the surface states using the Kronig–Penney model both for the semi-infinite and the infinite crystal model. Eldib[10] had also applied the Kronig–Penney model to one-dimensional crystal. He had calculated only the electronic energy bands for mono- and polyatomic crystals and compared his data with the one computed by using the linear combinations of atomic orbital methods.

In this paper, we shall use a one-dimensional Kronig–Penney model to represent the crystal potential field by a linear array of δ-function wells. By using essentially the electromagnetic field for p-polarized radiation, as given by Bagchi and Kar,[3] and also used by us previously,[4] we shall calculate the photoemission cross section. The initial state wave function will be the one deduced by Thapa and Kar.[11] The relevant matrix element then can be written as, using atomic units ($e = m = \hbar = 1$),

$$\begin{aligned}\langle\psi_f|H'|\psi_i\rangle &= \int_{-\infty}^{\infty} \psi_f^*(z) H' \psi_i(z) dz\,,\\ \langle\psi_f|H'|\psi_i\rangle &= \int_{-\infty}^{\infty} \left[\psi_f^*(z) A_\omega(z) \frac{d\psi_i}{dz} + \frac{1}{2}\psi_f^*(z) \frac{dA_\omega}{dz}\psi_i(z)\right] dz\,,\end{aligned} \tag{2}$$

using the commutation relation between A and p, with $A_\omega(z)$ being the vector potential for the photon with energy $\hbar\omega$.

The expressions for $A_\omega(z)$ are the same as given by Bagchi and Kar,[3] and may be written as

$$A_\omega(z) = \begin{cases} A_1\,, & z < -a/2\,,\\ \dfrac{A_1}{z/a + B_1}\,\dfrac{\varepsilon(\omega)}{1-\varepsilon(\omega)}\,, & -a/2 < z < a/2\,,\\ \varepsilon(\omega) A_1\,, & z > a/2\,,\end{cases} \tag{3}$$

with $\varepsilon(\omega)$ being the dielectric function and A_1 and B_1 are constants depending on $\varepsilon(\omega)$ and the angle of incidence. The surface region is $-a/2 \le z \le a/2$ where the dielectric function is a linearly interpolated one between the vacuum value and the bulk value.

In Eq. (2) above, $\psi_f(z)$ is the free electron final state wave function as given by the following expression:

$$\psi_f(z) = \begin{cases} (1/2\pi q)^{1/2}\,\dfrac{2q}{q+k_f}\,e^{ik_f z}\,, & z < 0\,,\\ (1/2\pi q)^{1/2}\left[e^{iqz} + \left(\dfrac{q-k_f}{q+k_f}\right)e^{-iqz}\right], & z > 0\,,\end{cases} \tag{4}$$

where $k_f^2 = 2E_f$, $q^2 = 2(E_f - V_0)$, and $E_f = E_i + \hbar\omega$.

To evaluate the initial state wave function $\psi_i(z)$, one generally solves the one-dimensional Schrödinger's equation which can be written as

$$\frac{d^2\psi(z)}{dz^2} + k_i^2\psi(z) = -2V(z)\psi(z)\,, \tag{5}$$

where $k_i^2 = 2E$ and $V(z)$ is the δ-function potential of the Kronig–Penney model.

We shall calculate $\psi_i(z)$ by matching the wave function and its derivative at $z = 0$. Let $\phi(z)$ denote the Bloch wave function deep in the metal and $\phi^*(z)$ the time reversal version of $\phi(z)$. The eigenfunction in the semi-infinite solid ($z < 0$) has been chosen to have the form

$$\psi_i(z) = \phi(z) - P\phi^*(z)\,, \tag{6}$$

where P is the reflection coefficient which was evaluated by matching the wave function and the slope at $z = 0$. One can then show that the initial state wave function for $z < 0$ may be written as

$$\psi_i(z) = (1 - iPe^{-i\delta}\sin\delta)e^{ik_iz} - (P - ie^{i\delta}\sin\delta)e^{-ik_iz}\,, \tag{7}$$

where

$$\cot\delta = -\frac{k_i}{g}$$

with g being the strength of the potential. The initial state wave function outside the metal ($z > 0$) is

$$\psi_i(z) = Te^{-\varkappa z}\,, \tag{8}$$

where T is the transmission coefficient across the boundary plane and

$$\varkappa^2 = 2(V_0 - E)\,, \tag{9}$$

V_0 being the step potential at the surface. By matching conditions at $z = 0$, we get

$$P = \frac{(\varkappa - ik_i) - (k_i - i\varkappa)e^{i\delta}\sin\delta}{(\varkappa - ik_i) + (k_i - i\varkappa)e^{-i\delta}\sin\delta}\,, \tag{10}$$

$$T = \frac{2k_i\sin 2\delta}{(\varkappa - ik_i) + (k_i - i\varkappa)e^{-i\delta}\sin\delta}\,. \tag{11}$$

The proper evaluation of P and T with the appropriate numerical values for other factors enables one to write explicitly the initial state wave function ψ_i. The photoemission cross section was calculated by using the formula

$$\frac{d\sigma}{d\Omega} = \frac{k^2}{\omega}\,|\langle\psi_f|H'|\psi_i\rangle|^2\,. \tag{12}$$

The matrix element $I = \langle\psi_f|H'|\psi_i\rangle$ in Eq. (12) can be written as

$$I = \int_{-\infty}^{-a/2} \psi_f^* A_\omega(z) \frac{d\psi_i}{dz}\, dz + \int_{-a/2}^{0} \psi_f^* A_\omega(z) \frac{d\psi_i}{dz}\, dz$$
$$+ \frac{1}{2} \int_{-a/2}^{0} \psi_f^* \frac{dA_\omega(z)}{dz} \psi_i dz + \int_{0}^{a/2} \psi_f^* A_\omega(z) \frac{d\psi_i}{dz} dz$$
$$+ \frac{1}{2} \int_{0}^{a/2} \psi_f^* \frac{dA_\omega(z)}{dz} \psi_i dz + \int_{a/2}^{\infty} \psi_f^* A_\omega(z) \frac{d\psi_i}{dz}\, dz\,. \qquad (13)$$

To calculate the photocurrent, these integrals were evaluated analytically, where possible, or numerically. To ensure convergence a factor of $e^{-\alpha|z|}$ was introduced for $z < 0$. This represents the effect of inelastic collisions. We have used complex dielectric functions corresponding to tungsten and silicon. The data for these were those given by Weaver[12] and Edwards.[13] Since it is a model calculation, we have chosen the same set of data (in a.u.) for these two cases: $E = 0.43$ eV, $\delta = -0.5753$, $g = 0.60$, and $\theta = 45°$.

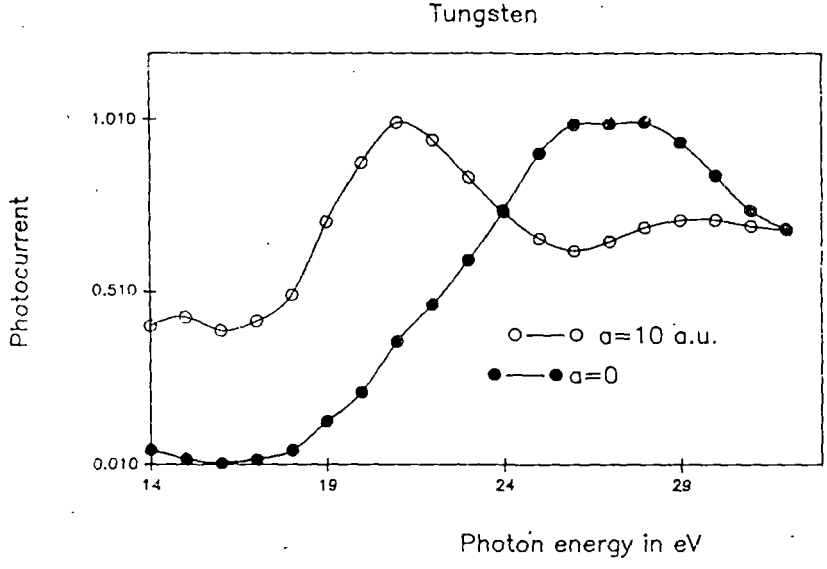

Fig. 1. Photocurrent against photon energy plots with tungsten dielectric functions for $a = 10$ a.u. and $a = 0$, i.e. with Fresnel field. The scales for the two curves are not the same; they have been so adjusted that the maxima for the two curves become comparable.

The results obtained with the dielectric function of tungsten for $\alpha = 0.5$ and $a = 10$ a.u. are shown in Fig. 1 (the curve with open circles). As expected, there is a minimum around the plasmon energy ($\hbar\omega_p$) which in this case is about 25 eV.

There is a peak below $\hbar\omega_p$ and another broad one above it. We also did a calculation without any surface region (Fig. 1 — the curve with closed circles) and again we find that the minimum at the plasmon energy is missing, but instead there is a maximum at 27 eV. Experimental observations of photocurrent from the tungsten (100) surface state did show a minimum at the $\hbar\omega_p$ and this supports our conclusion that the surface variation of the photon field is important in analyzing this type of spectrum.

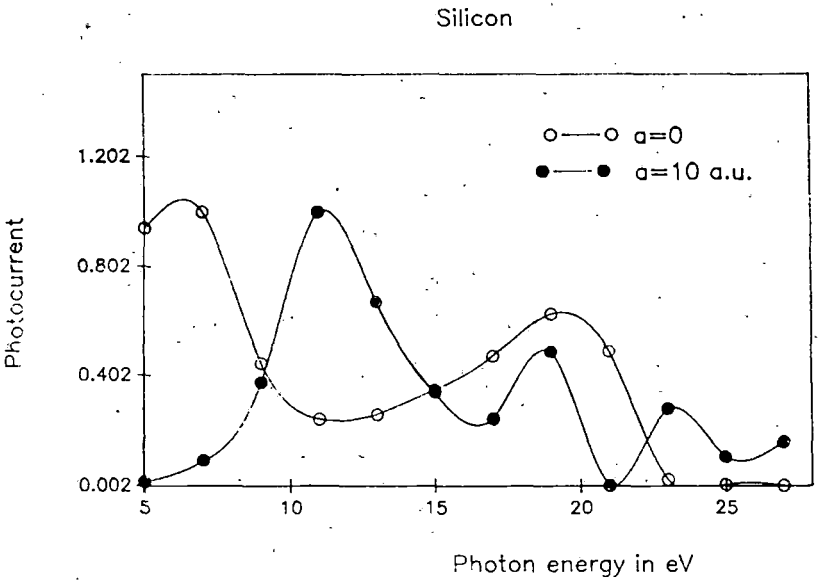

Fig. 2. Photocurrent against photon energy plots with silicon dielectric functions for $a = 10$ a.u. and $a = 0$, i.e. with Fresnel field. The scales for the two curves are not the same; they have been so adjusted that the maxima for the two curves become comparable.

We have also used this model in conjunction with the dielectric function $\varepsilon(\omega)$ for silicon as given by Edwards[12] which is a semiconductor and has a somewhat different dielectric response. With the same Kronig–Penney parameters and the same E, the results for $\alpha = 0.5$ and $a = 10$ a.u. are shown in Fig. 2 (the curve with filled circles). As in the other cases, there is a minimum at the plasmon energy around 16 eV. There is a maximum below $\hbar\omega_p$ and the current rises also beyond $\hbar\omega_p$. But in this case, we see another minimum which is at 21 eV. The reason for this can be traced to the behavior of $\varepsilon(\omega)$ for silicon which has instability in the region of 21 eV. As a result of this, the fields inside the solid become extremely small and, consequently, the photocurrent also shows a minimum. The photocurrent calculated with no surface region, i.e. with Fresnel fields (Fig. 2 — the plot with open circles) shows no minimum at 16 eV (the plasmon energy of silicon) and a

maximum at 21 eV. This, again, demonstrates that the behavior with and without the surface region is strikingly different.

A study of these cases shows that the surface variation of the photon field is important in calculating photoemission cross section, since neglecting it fails to reproduce the minimum at the plasmon energy. We also see that using dielectric functions corresponding to different elements changes the results. All of these point to the fact that a full fledged photoemission calculation should include the correct variation of photon field near the surface.

Acknowledgement

One of the authors (N.K.) acknowledges a research grant from the Council of Scientific and Industrial Research, India. The other author (R.K.T.) also acknowledges a grant from the Department of Atomic Energy, India.

References

1. D. R. Penn, *Phys. Rev. Lett.* **28**, 1041 (1972).
2. J. B. Pendry, *Surf. Sci.* **57**, 679 (1976).
3. A. Bagchi and N. Kar, *Phys. Rev.* **B18**, 5248 (1978).
4. P. Das, R. K. Thapa, and N. Kar, *Mod. Phys. Lett.* **B5**, 65 (1991).
5. W. Shockley, *Phys. Rev.* **56**, 317 (1939).
6. S. G. Davison and J. D. Levine, *Solid State Phys.* **25**, 2 (1970).
7. W. L. Schaich and N. W. Ashcroft, *Phys. Rev.* **B3**, 2452 (1971).
8. K. Mitchell, *Proc. Royal Soc. London, Ser.* **A146**, 443 (1934).
9. M. Steslicka, *Prog. Surf. Sci.* **5**, 157 (1974).
10. A. M. Eldib, H. F. Hassaon, and M. A. Mohmad, *J. Phys.* **C20**, 3011 (1987).
11. R. K. Thapa and N. Kar, *Indian J. Pure Appl. Phys.* **26**, 620 (1988).
12. J. Weaver, in *Handbook of Chemistry and Physics of Solids* (CRC Press, Boca Raton, Ohio, 1987) E-377.
13. D. F. Edwards, *Handbook of Optical Constants of Solids*, ed. E. P. Palik (Orlando, Academic, 1985) p. 555.